Title

Elemental changes and alteration recorded by basaltic drill core samples recovered from in situ temperatures up to 345°C in the active, seawater-recharged Reykjanes geothermal system, Iceland

Permalink

https://escholarship.org/uc/item/65b3p62g

Journal

Geochemistry Geophysics Geosystems, 17(11)

ISSN

1525-2027

Authors

Fowler, Andrew PG
Zierenberg, Robert A

Publication Date

2016-11-01

DOI

10.1002/2016gc006595

Peer reviewed

RESEARCH ARTICLE

Key Points:
- Lithologies originally emplaced on the seafloor integrate chemical changes from progressively advanced stages of alteration
- Alteration and elemental changes in Reykjanes drill cores are comparable to those reported from the deepest levels of in situ oceanic crust
- High-temperature alteration is not overprinted by retrograde alteration, in contrast to samples drilled from the ocean crust or ophiolites

Supporting Information:
- Supporting Information S1

Correspondence to:
A. P. G. Fowler,
apfowler@ucdavis.edu

Elemental changes and alteration recorded by basaltic drill core samples recovered from in situ temperatures up to 345°C in the active, seawater-recharged Reykjanes geothermal system, Iceland

Andrew P. G. Fowler[1] and Robert A. Zierenberg[1]

[1]Department of Earth and Planetary Sciences, University of California, Davis, California, USA

Abstract Hydrothermal activity results in element exchanges between seawater and oceanic crust that contribute to many aspects of ocean chemistry; therefore, improving knowledge of the associated chemical processes is of global significance. Hydrothermally altered basaltic drill core samples from the seawater-recharged Reykjanes geothermal system in Iceland record elemental gains and losses similar to those observed in samples of hydrothermally altered oceanic crust. At Reykjanes, rocks originally emplaced on the seafloor were buried by continued volcanism and subsided to the current depths (>2250 m below surface). These rocks integrate temperature-dependent elemental gains and losses from multiple stages of hydrothermal alteration that correspond to chemical exchanges observed in rocks from different crustal levels of submarine hydrothermal systems. Specifically, these lithologies have gained U, Mg, Zn, and Pb and have lost K, Rb, Ba, Cu, and light rare earth elements (La through Eu). Alteration and elemental gains and losses in lithologies emplaced on the seafloor can only be explained by a complex multistage hydrothermal alteration history. Reykjanes dolerite intrusions record alteration similar to that reported for the sheeted dike section of several examples of oceanic crust. Specifically, Reykjanes dolerites have lost K, Rb, Ba, and Pb, and gained Cu. The Reykjanes drill core samples provide a unique analog for seawater-oceanic crust reactions actively occurring at high temperatures (275–345°C) beneath a seafloor hydrothermal system.

1. Introduction

Drill core samples recovered by the Iceland Deep Drilling Project (IDDP) from the Reykjanes geothermal system in SW Iceland provide unique examples of in situ seawater-basalt reaction at elevated temperatures (275–345°C) and extreme depths (2245 and ~2570 m). The seawater-recharged Reykjanes geothermal system is located on the immediate onshore extension of the submarine Reykjanes Ridge (Figure 1). Prior to the discovery and direct observation of seafloor hydrothermal activity, the Reykjanes geothermal system was recognized as a useful analog for studying chemical exchange reactions between seawater and basalt resulting from seafloor hydrothermal activity [*Bischoff and Dickson*, 1975; *Elderfield et al.*, 1977; *Mottl and Holland*, 1978], when important differences in pressure are accounted for.

Alteration of oceanic crust by seawater is a critical planetary-scale geochemical process that affects seawater composition [*Hart*, 1970; *Elderfield et al.*, 1977; *Humphris and Thompson*, 1978a]. Drill core samples recovered by the Deep Sea Drilling Project (DSDP), Ocean Drilling Program (ODP), and Integrated Ocean Drilling Program (IODP), and sections of sheeted dikes tectonically uplifted and exposed on the East Pacific Rise at Hess Deep and Pito Deep have been essential for estimating the role of hydrothermal element fluxes between oceanic crust and the oceans in global geochemical cycles [*Staudigel et al.*, 1981a, 1981b; *Alt et al.*, 1986; *Verma*, 1992; *Mottl and Wheat*, 1994; *Staudigel et al.*, 1995, 1996; *Gillis*, 1996; *Alt and Teagle*, 1999; *Hart et al.*, 1999; *Laverne et al.*, 2001; *Wheat et al.*, 2002; *Bach et al.*, 2001, 2003; *Teagle et al.*, 2003; *Heft et al.*, 2008; *Alt et al.*, 2010; *Dekkers et al.*, 2014].

Owing to the expense and technical challenges of seafloor exploration and submarine drilling, drill core samples have been recovered from only four holes that penetrate greater than 1000 m into oceanic crust (DSDP/ODP Hole 504B, ODP/IODP Hole 1256D, ODP Hole 735B, and IODP Hole U1309D) [*Ildefonse et al.*, 2007]. Holes 735B and U1309D predominantly sampled gabbroic rocks that were tectonically uplifted and
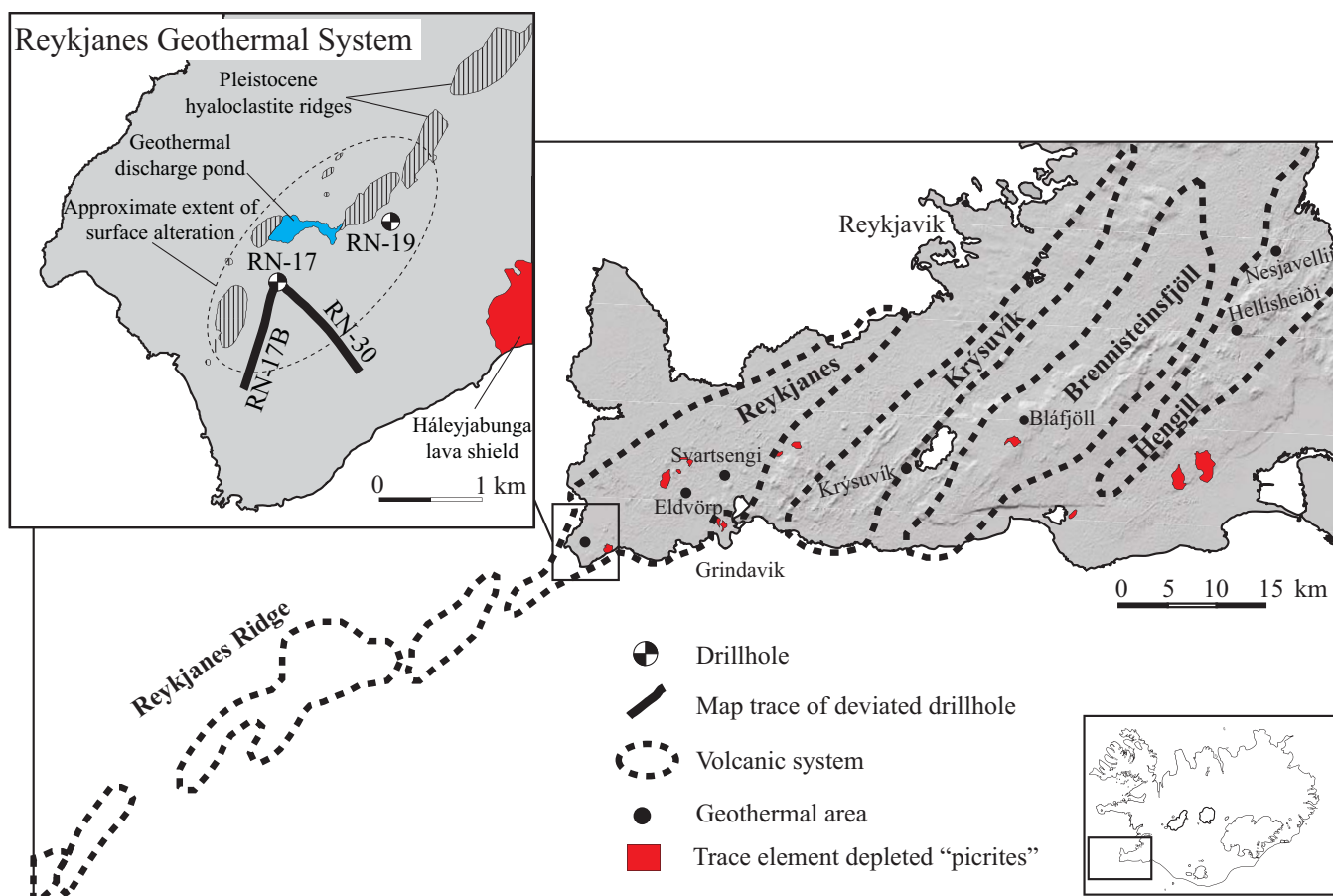
Figure 1. Location map of Reykjanes Peninsula volcanic systems and geothermal areas. Subaerial exposures of trace element depleted (TED) "picritic" basalts are indicated in red. Inset map shows the locations where drill core and drill cutting samples discussed in this study were collected. Modified from *Jakobsson et al.* [1978], *Sæmundsson* [1979], and *Einarsson and Sæmundsson* [1987].

exposed to later low-temperature alteration processes [*Bach et al.*, 2001; *Nozaka and Fryer*, 2011], and are not discussed further. Holes 504B and 1256D were completed in 5.9 and 15 Ma low-temperature oceanic crust that is no longer exposed to axial hydrothermal conditions. Thus, the maximum temperature measured in Hole 504B was 165°C [*Becker et al.*, 1989] and 67.5°C in Hole 1256D [*Teagle et al.*, 2006]. While samples from deep levels of oceanic crust exposed at Hess Deep, and drilled from Hole 504B and Hole 1256D, record early stage, high-temperature (>400°C) on-axis hydrothermal alteration, subsequent zeolite and prehnite mineralization suggests at least some geochemical influence from late-stage low-temperature alteration [*Alt et al.*, 1996; *Gillis*, 1996; *Alt et al.*, 2010]. Localized oxidation halos in the sheeted dike section exposed at Pito Deep indicate samples have undergone low-temperature weathering by seawater [*Gillis*, 1996; *Heft et al.*, 2008].

Lithology, alteration mineralogy, and temperature characteristics of the Reykjanes geothermal system are well characterized from the more than 30 wells that have been drilled for the production of geothermal energy, some to depths exceeding 3000 m. The majority of subsurface samples from these wells are returned as drill cuttings, which are of limited use for determining seawater-basalt element exchanges due to mixing of different lithologies and contamination of samples by drilling equipment [*Fowler and Zierenberg*, 2016]. Recently, the Iceland Deep Drilling Project (IDDP) recovered spot drill cores to test newly designed drilling equipment during the drilling of three new geothermal wells (RN-17B, RN-19, and RN-30) in the Reykjanes geothermal system. The spot cores were recovered from true vertical depths ranging between ~2245 and ~2570 m and in situ temperatures ranging from ~275 to 345°C [*Friðleifsson et al.*, 2005; *Friðleifsson and Richter*, 2010; *Friðleifsson et al.*, 2014; *Fowler et al.*, 2015].

The lithologies recovered in the RN-17B core include pillow basalts, hyaloclastite breccia, lithic breccia, and basaltic sandstone and are consistent with original emplacement on the seafloor within the axial volcanic zone [*Fowler et al.*, 2015]. The cored interval has undergone high-temperature (>400°C) alteration by seawater resulting in the formation of secondary calcic plagioclase and hydrothermal hornblende, followed by cooling to temperatures between 345 and 400°C recorded by epidote vein-hosted fluid inclusions [*Fowler et al.*, 2015]. The alteration mineral assemblage in the RN-17B core is similar to high-temperature alteration preserved in the lower sheeted dikes (1500–2111 m below seafloor [mbsf]) in Hole 504B [*Alt*, 1995; *Fowler et al.*, 2015]. The original rocks in the RN-19 and RN-30 cores from the Reykjanes Peninsula consist of a series of crystalline intrusive basalts including chilled margins characteristic of sheeted dike samples recovered from in situ oceanic crust. These preliminary IDDP drill cores collected at Reykjanes provide the first deep (>1000 m) oceanic crust samples recovered from a zone that is actively undergoing high-temperature (>275°C) alteration by seawater.

The objective of this study is to document seawater-basalt element exchanges recorded by the Reykjanes IDDP cores. Whole-rock hydrothermal element gains and losses are determined by comparing the IDDP samples to unaltered equivalents. We compare compositional changes in the Reykjanes drill cores to those in hydrothermally altered samples dredged from the seafloor and drilled from in situ oceanic crust. We show that the Reykjanes drill cores originally emplaced on the seafloor record the integrated effects of advancing stages of alteration, and preserve some aspects of earlier low-temperature weathering and alteration. In contrast, dolerite dikes intruded at depth solely record high-temperature alteration similar to sheeted dike samples recovered from in situ oceanic crust, although differ in that there is no evidence of overprinting by subsequent low-temperature alteration.

1.1. Geology of the Reykjanes Peninsula

The combination of volcanic activity and tectonic extension has produced several high-temperature geothermal areas along the Reykjanes Peninsula, of which the Reykjanes geothermal system is at the westernmost tip [*Jakobsson et al.*, 1978; *Arnórsson*, 1995]. Fluids in the Reykjanes geothermal system are composed of seawater chemically modified by boiling and reaction with the basaltic host rock [*Tómasson and Kristmannsdóttir*, 1972; *Arnórsson*, 1978, 1995; *Freedman et al.*, 2009]. Deep fluid samples have dissolved metal and major element compositions similar to typical seafloor black smoker fluids [*Hardardóttir et al.*, 2009, 2012]. Oxygen and deuterium isotope values of fluids and alteration minerals suggest that meteoric fluids infiltrated the system and mixed with seawater sometime in the past [*Ólafsson and Riley*, 1978; *Sveinbjörnsdóttir et al.*, 1986; *Lonker et al.*, 1993; *Pope et al.*, 2009; *Marks et al.*, 2015]. The Sr isotope (^{87}Sr/^{86}Sr) values of alteration minerals coupled with elevated fluid inclusion salinities indicate that even during periods of increased meteoric fluid infiltration, seawater has remained the dominant component of fluids and increasingly so with depth [*Franzson et al.*, 2002; *Fowler et al.*, 2015; *Marks et al.*, 2015].

Below 1200 m in the Reykjanes geothermal system, fluids increase in temperature with depth, are freely convecting, but are not boiling [*Ármannsson*, 2016]. Key alteration mineral zones change as a function of increasing depth and temperature [*Tómasson and Kristmannsdóttir*, 1972; *Lonker et al.*, 1993; *Marks et al.*, 2010, 2011]. A monotonic increase in temperature with depth and the convex-upward shape of alteration mineral isograds indicate the Reykjanes geothermal system is a zone of focused hydrothermal up-flow, and lateral fluid flow is of little significance to alteration and fluid characteristics at currently explored depths [e.g., *Marks et al.*, 2015].

The Reykjanes Peninsula is divided into five neo-volcanic fissure swarms (Reykjanes, Grindavík, Krýsuvík, Bláfjöll, and Hengill), expressed in an en echelon arrangement of postglacial eruptions [*Jakobsson et al.*, 1978; *Clifton and Kattenhorn*, 2006]. Basalts in the neo-volcanic fissure swarms are indistinguishable in terms of petrology and major element chemistry [*Jakobsson et al.*, 1978]. The postglacial neo-volcanic fissure swarms are linked to four volcanic systems (Reykjanes, Krísuvik, Brennisteinsfjöll, and Hengill), each with a unique magma supply, and prolonged volcanic history [*Sæmundsson*, 1979; *Einarsson and Sæmundsson*, 1987].

Submarine Reykjanes Ridge and subaerial Reykjanes Peninsula basalts differ isotopically and compositionally from normal mid-ocean ridge basalts and are compositionally more heterogeneous [*Schilling*, 1973; *Hart et al.*, 1973; *Murton et al.*, 2002; *Koornneef et al.*, 2012]. Surface samples from the Reykjanes Peninsula range petrographically from picritic basalts to tholeiitic basalts, with intermediate and acid rocks identified only in

the easternmost Hengill volcanic system [*Jakobsson et al.*, 1978]. Tholeiitic basalts are the dominant exposed rock type, while picritic basalts account for $<2\%$ of the erupted volume exposed on the western Reykjanes Peninsula [*Jackobsson et al.*, 1978] (Figure 1). The picritic basalt parental liquid was likely a high-MgO (11–13 wt %) primitive basalt rather than a true picritic liquid (MgO >18 wt %), considering the picritic basalts contain high and variable cumulate olivine [*Gee et al.*, 1998; *Revillon et al.*, 1999].

Reykjanes Peninsula tholeiitic and "picritic" basalts have distinct incompatible and moderately incompatible element ratios, with few intermediate compositions [*Gee et al.*, 1998]. The high-MgO "picritic" basalts in the Reykjanes volcanic system are defined by Nb/Zr ratios <0.07, have low incompatible element abundances, and are referred to here as "trace element depleted" after *Gee et al.* [1998]. The more voluminous and more evolved tholeiitic basalts (MgO generally $<8\%$) are defined by Nb/Zr ratios >0.07, and have higher incompatible element abundances relative to the trace element depleted lavas, and are referred to here as "trace element enriched" [*Gee et al.*, 1998; *Kokfelt*, 2006; *Peate et al.*, 2009]. While the trace element depleted (TED) and trace element enriched (TEE) basalts are generally distinguishable based on $^{87}Sr/^{86}Sr$, $^{206}Pb/^{204}Pb$, and $^{143}Nd/^{144}Nd$ isotopic ratios [*Zindler et al.*, 1979; *Gee et al.*, 1998], there is overlap [*Thirlwall et al.*, 2004]. The TED basalts generally have lower $^{87}Sr/^{86}Sr$ (0.702888–0.703556) and $^{206}Pb/^{204}Pb$ (18.1564–18.7787), and higher $^{143}Nd/^{144}Nd$ (0.513032–0.513148). TEE basalts generally have higher $^{87}Sr/^{86}Sr$ (0.703093–0.70336) and $^{206}Pb/^{204}Pb$ (18.554–18.9707), and lower $^{143}Nd/^{144}Nd$ (0.512964–0.513077) [*Zindler et al.*, 1979; *Elliott et al.*, 1991; *Hemond et al.*, 1993; *Gee et al.*, 1998; *Revillon et al.*, 1999; *Chauvel and Hémond*, 2000; *Kempton et al.*, 2000; *Skovgaard et al.*, 2001; *Thirlwall et al.*, 2004; *Kokfelt*, 2006; *Brandon et al.*, 2007; *Nielsen et al.*, 2007; *Peate et al.*, 2009; *Martin and Sigmarsson*, 2010; *Koornneef et al.*, 2012].

Isotopic and trace element differences between the TEE and TED basalts cannot be explained by fractional crystallization alone [*Wood et al.*, 1979; *Hemond et al.*, 1993]. The differences between TEE and TED basalts on the Reykjanes Peninsula have been explained by various combinations of mantle source heterogeneity [*Zindler et al.*, 1979], mixing of at least two components [*Chauvel and Hemond*, 2000; *Fitton*, 2003; *Kokfelt*, 2006; *Koornneef et al.*, 2012], mixing of more than two components [*Hanan and Schilling*, 1977; *Thirlwall et al.*, 2004; *Peate et al.*, 2009, 2010], assimilation of hydrothermally altered crust [*Oskarsson et al.*, 1985; *Hemond et al.*, 1993; *Gee et al.*, 1998; *Kokfelt*, 2006], and mixing of melts that were extracted at different crustal levels [*Koornneef et al.*, 2012].

2. Materials and Methods

2.1. Core Drilling

IDDP and the geothermal field operator, HS Orka hf, provided samples of drill core from RN-17B, RN-19, and RN-30 (Figure 1 and Table 1). Coring was funded by the International Continental Scientific Drilling Program (ICDP) to test coring bit technology for a future IDDP attempt to obtain drill core from portions of the geothermal system hosting supercritical fluids [*Friðleifsson and Richter*, 2010; *Friðleifsson et al.*, 2014]. Wells chosen for coring were determined by the field operator.

The 4 inch diameter IDDP drill cores were obtained during or immediately after the rotary drilling of new geothermal production wells using freshwater as the drilling fluid; therefore, contamination of the core by scale minerals from previously produced fluids does not contribute to sample contamination. The RN-19 core was drilled using a Baker-Hughes PDC core-bit, with near 100% recovery (2.7 m) before termination of the coring run due to a suspected jammed core barrel [*Friðleifsson and Richter*, 2010]. The core apparently jammed in the core barrel when it broke along a high-angle chlorite-actinolite lined fracture at the base of the recovered core [*Friðleifsson and Richter*, 2010]. The RN-17B and RN-30 cores were obtained using a core-bit and core barrels specially designed for scientific drilling into extreme high-temperature conditions [*Skinner et al.*, 2010].

RN-19 is a near-vertical geothermal well located on the eastern edge of the main geothermal production area. RN-17B and RN-30 were drilled from the same pad and are deviated at depth to the SSW and SE, respectively (Figure 1), both at 35° from vertical. Because wells RN-17B and RN-30 are not vertical, the true vertical depth differs from the downhole depth. Sample labels and depths used in this study refer to downhole depth unless specifically stated. The 2.7 m long RN-19 core was recovered in April 2005 at a depth of $\sim$2245 m, where the in situ temperature was 275°C. It is composed of a coarse crystalline dolerite intrusion interpreted to come from a sheeted dike complex [*Friðleifsson et al.*, 2005; *Mortensen et al.*, 2006; *Friðleifsson*

Table 1. Major and Trace Element Values for Rock Samples From IDDP Drill Cores

Sample	2245	<2510.5-1	<2510.5-2[a]	2510.5	2512.53[a]	2516.06	2519.8
Drill Hole	RN-19 Core	RN-30	RN-30	RN-30	RN-30	RN-30	RN-30
Lithology	Dolerite	Hyaloclastite	Hyaloclastite	Dolerite	Dolerite	Dolerite	Dolerite
Major Elements by XRF (wt %)							
SiO_2	48.91	70.79	57.14	48.23	49.20	49.49	49.04
TiO_2	0.56	0.84	1.07	1.69	1.76	0.48	1.68
Al_2O_3	19.05	8.63	9.38	13.90	13.67	13.86	13.67
FeO*	8.31	4.00	8.03	13.13	13.04	9.09	12.87
MgO	6.34	3.10	8.92	7.01	6.86	9.65	6.89
MnO	0.14	0.06	0.11	0.20	0.22	0.17	0.22
CaO	13.99	6.64	4.54	11.56	11.16	13.34	11.48
Na_2O	1.76	2.41	0.83	2.50	2.58	1.36	2.30
K_2O	0.04	0.06	0.15	0.05	0.05	<0.031	0.04
P_2O_5	0.02	0.48	0.18	0.16	0.16	0.02	0.17
Total	99.12	97.01	90.35	98.43	98.70	97.46	98.36
LOI (%)	<1.0	1.48	4.88	<1.0	<1.0	1.60	<1.0
Trace Elements by XRF (ppm)							
V	232	181	198	374	336	220	383
Cr	97	204	120	112	221	251	87
Ni	69	65	69	71	101	105	63
Cu	144	53	423	149	156	68	182
Zn	59	29	95	109	95	53	106
Trace Elements by ICP-MS (ppm)							
Sc	36.45	21.56	27.85	46.72	44.57	44.91	45.87
Rb	0.65	0.83	2.55	0.23	0.27	0.10	0.25
Sr	94.18	135.63	81.06	161.12	152.07	88.17	150.49
Y	12.13	19.76	19.84	27.44	28.12	12.73	28.13
Zr	19.95	43.68	56.97	87.17	89.65	16.80	90.48
Nb	0.98	5.37	7.09	9.37	9.75	0.99	9.92
Cs	0.02	<0.014	0.03	<0.014	<0.014	<0.014	<0.014
Ba	10.07	54.14	100.52	31.57	33.35	10.81	31.39
La	1.07	6.32	5.10	7.34	7.65	0.95	7.70
Ce	2.98	13.23	12.75	17.79	18.47	2.57	18.55
Pr	0.49	1.88	1.85	2.60	2.67	0.44	2.68
Nd	2.67	9.05	8.91	12.30	12.51	2.42	12.83
Sm	1.07	2.43	2.57	3.59	3.79	1.00	3.83
Eu	0.47	1.01	0.86	1.36	1.37	0.46	1.41
Gd	1.56	3.02	3.16	4.46	4.54	1.59	4.57
Tb	0.31	0.51	0.56	0.81	0.83	0.32	0.83
Dy	2.18	3.17	3.49	5.22	5.30	2.29	5.41
Ho	0.47	0.65	0.74	1.11	1.14	0.50	1.13
Er	1.38	1.73	2.01	3.10	3.16	1.40	3.16
Tm	0.20	0.24	0.29	0.44	0.45	0.21	0.44
Yb	1.29	1.41	1.76	2.72	2.84	1.37	2.75
Lu	0.20	0.22	0.27	0.41	0.43	0.21	0.44
Hf	0.59	1.17	1.52	2.35	2.41	0.54	2.36
Ta	0.08	0.38	0.48	0.64	0.68	0.09	0.67
Pb	<0.204	0.72	0.39	<0.204	<0.204	<0.204	<0.204
Th	0.09	0.24	0.25	0.45	0.48	0.04	0.46
U	0.02	0.77	0.12	0.13	0.14	0.01	0.15
Nb/Zr	0.05	0.12	0.12	0.11	0.11	0.06	0.11
Y/Zr	0.61	0.45	0.35	0.31	0.31	0.76	0.31
Protolith[d]	TED	TEE	TEE	TEE	TEE	TED	TEE

Sample	2521.75	2526.14	2530.24	2798.64	2800.05	2800.35[a]	2800.75
Drill Hole	RN-30	RN-30	RN-30	RN-17B	RN-17B	RN-17B	RN-17B
Lithology	Dolerite	Dolerite	Dolerite	Hyaloclastite	Hyaloclastite	Basalt Pillow	Volcanic Sandstone
Major Elements by XRF (wt %)							
SiO_2	49.18	49.30	48.45	53.97	42.91	44.53	50.56
TiO_2	1.71	0.60	1.73	1.05	1.43	1.20	1.08
Al_2O_3	13.66	14.61	13.77	11.89	14.16	14.92	12.82
FeO*	12.85	9.66	13.25	9.47	12.15	11.54	10.12
MgO	6.88	9.05	6.88	7.68	10.72	10.99	8.38
MnO	0.21	0.17	0.22	0.25	0.27	0.23	0.25
CaO	11.73	13.90	12.11	9.68	12.44	8.69	11.23
Na_2O	2.10	1.45	2.08	4.21	1.01	2.38	3.28
K_2O	0.04	<0.031	0.03	0.04	0.05	0.05	0.04
P_2O_5	0.18	0.03	0.16	0.09	0.12	0.10	0.10

Table 1. (continued)

Sample	2521.75	2526.14	2530.24	2798.64	2800.05	2800.35[a]	2800.75
Drill Hole	RN-30	RN-30	RN-30	RN-17B	RN-17B	RN-17B	RN-17B
Lithology	Dolerite	Dolerite	Dolerite	Hyaloclastite	Hyaloclastite	Basalt Pillow	Volcanic Sandstone
Total	98.54	98.77	98.68	98.33	95.26	94.63	97.86
LOI (%)	1.07	1.09	1.38	<1.0	3.42	4.43	1.72
Trace Elements by XRF (ppm)							
V	366	364	384	215	366	349	265
Cr	102	101	94	141	114	93	290
Ni	67	66	66	70	121	72	77
Cu	182	166	158	<7.4	8	<7.4	<7.4
Zn	100	82	92	151	184	179	142
Trace Elements by ICP-MS (ppm)							
Sc	44.99	46.36	45.90	42.65	50.69	43.31	39.74
Rb	0.26	0.09	0.08	0.30	0.49	0.59	0.45
Sr	131.36	70.94	151.63	66.13	130.60	71.88	113.43
Y	30.05	15.56	28.03	19.58	25.37	28.00	21.96
Zr	97.66	21.57	87.27	49.36	68.87	57.91	55.98
Nb	10.54	1.26	9.45	3.37	5.84	4.82	5.04
Cs	<0.014	<0.014	<0.014	<0.014	0.02	0.02	0.01
Ba	29.57	6.98	18.36	8.15	9.50	20.28	12.24
La	8.17	1.20	7.34	1.54	1.99	6.53	4.87
Ce	19.89	3.28	17.76	4.58	5.55	15.92	11.26
Pr	2.89	0.54	2.56	0.81	0.95	2.37	1.66
Nd	13.47	3.11	12.26	4.51	5.20	11.46	7.95
Sm	4.03	1.18	3.60	1.80	2.23	3.40	2.53
Eu	1.49	0.56	1.37	0.48	0.82	1.41	1.06
Gd	4.85	1.93	4.48	2.70	3.42	4.32	3.34
Tb	0.88	0.39	0.80	0.52	0.67	0.76	0.61
Dy	5.59	2.74	5.25	3.66	4.85	5.07	4.11
Ho	1.19	0.61	1.12	0.80	1.05	1.09	0.88
Er	3.30	1.76	3.04	2.30	2.92	3.07	2.46
Tm	0.49	0.26	0.43	0.33	0.43	0.45	0.35
Yb	2.98	1.64	2.74	2.11	2.62	2.87	2.19
Lu	0.46	0.26	0.42	0.33	0.40	0.46	0.34
Hf	2.59	0.69	2.36	1.47	1.97	1.68	1.61
Ta	0.72	0.11	0.64	0.22	0.38	0.33	0.33
Pb	0.21	<0.204	0.27	0.50	0.82	0.72	0.81
Th	0.51	0.06	0.45	0.21	0.37	0.33	0.46
U	0.15	0.02	0.14	0.08	0.10	0.11	0.24
Nb/Zr	0.11	0.06	0.11	0.07	0.08	0.08	0.09
Y/Zr	0.31	0.72	0.32	0.40	0.37	0.48	0.39
Protolith[d]	TEE	TED	TEE	TEE	TEE	TEE	TEE

Sample	2802.90	2804.50	2804.80	2806.00	2807.10	2807.33	Detection[b]	Precision[c]
Drill Hole	RN-17B	RN-17B	RN-17B	RN-17B	RN-17B	RN-17B	Limit	(% RSD)
Lithology	Lithic Breccia	Lithic Breccia	Lithic Breccia	Hyaloclastite	Volcanic Sandstone	Basalt Pillow		
Major Elements by XRF (wt %)								
SiO_2	50.76	46.41	45.28	49.12	50.66	45.91	<0.58	<0.01
TiO_2	0.55	0.61	0.57	1.75	1.75	1.45	<0.017	0.4
Al_2O_3	15.03	14.47	15.05	12.76	12.21	14.81	<0.16	0.1
FeO*	8.27	8.66	9.84	10.19	10.72	11.04	<0.2	0.20
MgO	7.60	9.46	8.36	8.68	7.80	8.59	<0.076	1.4
MnO	0.20	0.22	0.24	0.22	0.24	0.23	<0.002	0.4
CaO	12.03	15.42	16.38	11.66	10.49	11.76	<0.064	0.2
Na_2O	3.18	0.97	0.82	2.75	3.29	1.85	<0.045	1.3
K_2O	0.04	0.05	0.04	0.04	0.04	0.05	<0.031	0.2
P_2O_5	0.04	0.04	0.03	0.21	0.21	0.15	<0.005	0.3
Total	97.70	96.31	96.61	97.38	97.41	95.84		
LOI (%)	1.23	2.52	2.49	2.25	2.12	3.29	<1.0	
Trace Elements by XRF (ppm)								
V	216	244	238	326	327	339	<5.0	7.0
Cr	389	428	415	252	209	163	<3.0	5.0
Ni	137	155	135	109	97	81	<3.5	<1.0
Cu	<7.4	<7.4	<7.4	<7.4	19	66	<7.4	3.0
Zn	140	142	142	143	160	176	<3.3	1.0
Trace Elements by ICP-MS (ppm)								
Sc	37.91	44.99	42.37	38.06	36.89	43.97	<1.6	0.82
Rb	0.35	0.71	0.56	0.46	0.37	0.44	<0.057	1.06
Sr	136.61	132.72	139.64	107.25	99.95	125.45	<0.115	0.62

Table 1. (continued)

Sample	2802.90	2804.50	2804.80	2806.00	2807.10	2807.33	Detection[b]	Precision[c]
Drill Hole	RN-17B	RN-17B	RN-17B	RN-17B	RN-17B	RN-17B	Limit	(% RSD)
Lithology	Lithic Breccia	Lithic Breccia	Lithic Breccia	Hyaloclastite	Volcanic Sandstone	Basalt Pillow		
Y	14.89	15.76	15.88	29.49	29.04	30.81	<0.015	0.61
Zr	21.29	23.48	21.27	104.92	104.49	82.87	<0.059	0.57
Nb	1.35	1.13	0.95	11.49	11.83	8.25	<0.018	0.70
Cs	<0.014	0.02	0.01	<0.014	<0.014	0.01	<0.014	1.91
Ba	12.09	13.42	9.33	18.23	17.46	18.22	<0.258	0.65
La	1.30	1.03	0.99	10.12	11.23	6.68	<0.007	0.66
Ce	3.41	2.78	2.69	23.03	24.70	17.09	<0.012	0.60
Pr	0.56	0.48	0.48	3.29	3.45	2.60	<0.009	0.58
Nd	3.03	2.77	2.80	15.15	15.80	12.45	<0.045	0.79
Sm	1.18	1.20	1.25	4.38	4.41	3.75	<0.014	1.02
Eu	0.46	0.56	0.65	1.92	1.75	1.51	<0.010	1.23
Gd	1.85	1.90	2.04	5.13	5.19	4.76	<0.026	0.76
Tb	0.37	0.39	0.40	0.90	0.89	0.86	<0.007	0.97
Dy	2.63	2.80	2.85	5.69	5.69	5.70	<0.024	0.94
Ho	0.58	0.61	0.63	1.18	1.17	1.22	<0.006	0.82
Er	1.66	1.77	1.78	3.19	3.09	3.34	<0.021	1.19
Tm	0.24	0.26	0.27	0.45	0.45	0.49	<0.006	1.02
Yb	1.55	1.71	1.62	2.76	2.71	3.08	<0.023	0.79
Lu	0.24	0.27	0.25	0.43	0.41	0.48	<0.007	1.45
Hf	0.66	0.76	0.70	2.85	2.82	2.31	<0.032	0.90
Ta	0.08	0.07	0.06	0.77	0.78	0.54	<0.014	1.40
Pb	0.64	0.80	0.93	0.64	0.70	0.98	<0.204	3.60
Th	0.08	0.11	0.08	0.85	0.86	0.59	<0.009	1.00
U	0.22	0.07	0.06	1.13	0.56	0.20	<0.014	1.42
Nb/Zr	0.06	0.05	0.04	0.11	0.11	0.10		
Y/Zr	0.70	0.67	0.75	0.28	0.28	0.37		
Protolith[d]	TED	TED	TED	TEE	TEE	TEE		

[a]Values from *Fowler and Zierenberg* [2016].

[b]The limit of determination (LOD) for XRF measurements is the 2-sigma limit determined from analyzing 250 repeat experiments over 14 months by Washington State University (WSU) GeoAnalytical Lab. LOD for ICP-MS is the concentration equivalent of the analytical blank + 3 times the standard deviation of the concentration equivalent of replicate measurements of the analytical blank. Note that values approaching the LOD have associated errors of approximately ±100%.

[c]Precision is the % relative standard deviation (RSD; 1 sigma) based on replicate measurements of WSU in-house basalt standard BCR-C (n = 7 for XRF; n = 54 for ICP-MS). Cu %RSD is based on n = 7 XRF replicate measurements of granodiorite standard GSP-1.

[d]TEE = trace element enriched (Nb/Zr < 0.07); TED = trace element depleted (Nb/Zr > 0.07) as defined by *Gee et al.* [1998] for the Reykjanes Peninsula.

and Richter, 2010]. The 9.3 m RN-17B core was recovered in November 2008 at a downhole depth of 2798.5 m (true vertical depth ∼2560 m) and an in situ temperature of 345°C. The RN-17B core is composed of basalt pillows, hyaloclastite, lithic breccia, and volcanic sandstone. Three sequential cores totaling 22.5 m from RN-30 were recovered in May 2011 at a downhole depth starting at 2510.3 m (true vertical depth ∼2250 m), an in situ temperature 345°C [*Ármannsson*, 2016], and are composed of a series of fine to coarse crystalline dolerite intrusions of basaltic composition.

2.1.1. RN-19 Drill Core

The RN-19 drill core is composed of a homogenous coarse-grained dolerite with unaltered primary clinopyroxene and plagioclase (Figure 2A), and the mesostasis entirely altered to chlorite + actinolite (Figure 2B) [*Friðleifsson et al.*, 2005; *Friðleifsson and Richter*, 2010]. The core is cut by sparse 1–2 mm wide chlorite-actinolite veins. It is unclear whether the RN-19 dolerite is a sill or dike as no chilled margins are present and only a portion of the intrusion was recovered, although it is interpreted to come from a sheeted dike complex [*Friðleifsson and Richter*, 2010]. Xenocrystic plagioclase glomerocrysts are common in thin section (Figure 2B). Primary clinopyroxene and plagioclase host extensive secondary fluid inclusions in healed microfractures and cleavage planes (Figures 2A and 2B). Multiple generations of cross-cutting secondary fluid inclusion suites are present, some are entirely vapor dominated, some are liquid dominated, and some include both liquid and vapor dominated inclusions within the same healed fracture. Fluid inclusions are <5 μm in size, range from elongate to equant in shape, and have vapor bubbles ranging from ∼30 to >90% of the inclusion volume. Titanomagnetite and clinopyroxene are commonly altered to chlorite + actinolite along crystal margins (Figures 2B and 2C).
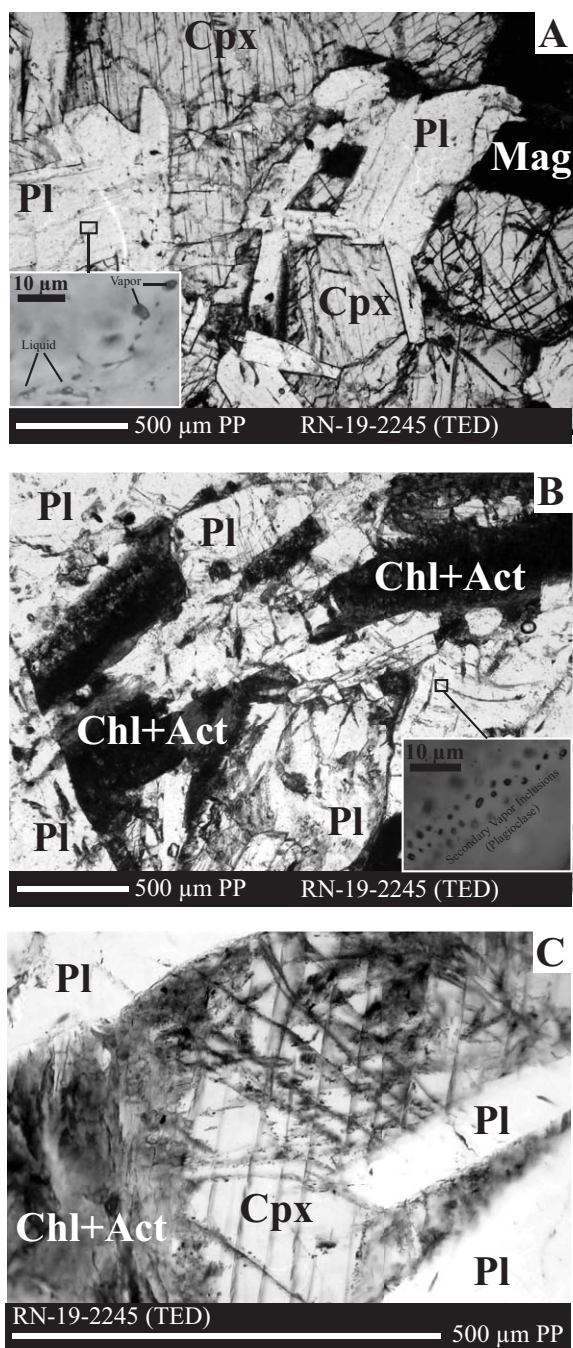
Figure 2. Plane polarized light images of a sample from 2245 m in Reykjanes drill core RN-19. (a) Primary igneous plagioclase (Pl), clinopyroxene (Cpx), and titanomagnetite (Mag) is preserved, inset photo shows small (<10 μm) liquid and vapor dominated fluid inclusions in healed fractures and cleavage planes within plagioclase. (b) Cumulate plagioclase glomercrysts that are common in the RN-19 core, inset photo shows secondary vapor fluid inclusions in a healed plagioclase fracture. Chlorite (Chl) and actinolite (Act) partially replace (b) titanomagnetite and (c) clinopyroxene.

2.1.2. RN-17B Drill Core

Detailed lithological and petrological descriptions of the RN-17B core are provided elsewhere [*Friðleifsson et al.*, 2005; *Friðleifsson and Richter*, 2010; *Fowler et al.*, 2015]. Lithologies preserved in the RN-17B core consist entirely of submarine basalt pillows, lithic breccia, hyaloclastite breccia, and basaltic sandstone similar to deposits observed along the axial ridges of the submarine Reykjanes Ridge [i.e., *Parson et al.*, 1993]. The rocks were subsequently buried by ongoing volcanic activity and subsided to current depths [*Friðleifsson and Richter*, 2010; *Fowler et al.*, 2015]. *Fowler et al.* [2015] describe alteration in the RN-17B core as follows. Hyaloclastite shards and pillow/clast rims originally composed of glass are present in hyaloclastite, lithic breccia, and sandstone units and are altered to brown hydrothermal hornblende surrounded by an albite-filled matrix. Crystalline clasts in clast-supported breccias are composed of uralitized clinopyroxene and plagioclase laths replaced by intergrowths of albite and calcic plagioclase. Actinolite, albite, chlorite, and epidote commonly fill void spaces and persist in the interiors of large crystalline clasts and basalt pillows. Minor secondary phases include pyrite, Fe-oxide, and titanite. Later epidote veins ($\pm$ pyrite $\pm$ actinolite) crosscut lithologies; quartz-bearing veins are absent in the cored interval. The RN-17B rocks are pervasively altered to a disequilibrium assemblage including both greenschist and amphibolite grade alteration minerals, and no primary igneous minerals persist.

The alteration history recorded in the RN-17B core, a sidetrack of hole RN-17, provides a very different picture of alteration compared to investigation of cuttings from RN-17 and RN-17B [*Marks et al.*, 2010; *Fowler and Zierenberg*, 2016]. Geochemical variations in RN-17 and RN-17B drill cuttings analyzed at 50 m depth intervals from downhole depths ranging between 350 and 3050 m [*Marks et al.*, 2010] are relatively minor compared to the variations seen in the RN-17B core, particularly for depths below 2000 m where intrusive rocks predominate [*Fowler and Zierenberg*, 2016]. Based on the relatively unaltered nature of the cuttings and oxygen and strontium isotope profiles showing little downhole variation below 2000 m, the impression is that the Reykjanes system is rock dominated with abundant intervals of relatively unaltered rock, and fluid flow is mostly controlled by infrequent fractures [*Marks et al.*, 2015]. In stark contrast, core RN-17B shows pervasive alteration and much larger variations in chemical composition, including zones

of Na addition and adjacent zones of Na depletion [*Fowler and Zierenberg*, 2016]. The coarse-grained cuttings that are routinely analyzed in order to infer downhole lithology and alteration are clearly biased by selective recovery of relatively unaltered rock and resistant alteration minerals, especially quartz and epidote, and caution should be used when inferring chemical exchange based on drill cuttings [*Fowler and Zierenberg*, 2016].

2.1.3. RN-30 Drill Core

We provide a detailed RN-30 core log as an electronic appendix. Building on *Friðleifsson*'s [2011] preliminary description of the RN-30 cores, we find the RN-30 drill cores consist of four to six dolerite intrusions of basaltic composition overlain by drill-rounded cobbles from a hyaloclastite deposit and hydrothermally altered fine-grained basalt that sloughed from higher levels of the borehole (Figure 3). The true number of intrusions is unknown owing to uncertainties about the relationships of the oldest intrusions to each other; they may be the same intrusion repeatedly intersected by younger intrusions, or different intrusions. The number of intrusions is also obscured by a tectonically fractured zone between ~2520 and 2524 m. All of the intrusions are intersected by numerous veins of chlorite ± amphibole, pyrite and chalcopyrite, and other <1 mm wide veins of chlorite + amphibole + quartz. Intrusion 1E (Figure 3) is intersected by several 1–2 mm wide epidote (±quartz?) veins. Three chilled margins and the epidote veins trend between 45° and 55° to the core axis. The core was drilled 35° from vertical suggesting the intrusions were likely to have been emplaced near vertically as dikes, but may have been intruded horizontally as sills, or at some angle between the two. A review by *Gudmundsson et al.* [2014] suggests that both dikes and sills are relatively common in Iceland; thus, a distinction cannot be conclusively made.

Here we distinguish RN-30 dolerites as having a TEE or TED precursor on the basis of our Nb/Zr and Y/Zr analyses (see section 3.1), following the classification of *Gee et al.* [1998]. TEE dolerites (intrusions 1A through 1E; Figure 3) contain plagioclase laths up to 1 mm long with an ophitic to subophitic texture, primary igneous minerals are heavily fractured, and alteration of primary igneous minerals is generally more advanced than for TED dolerites (Figure 4A). The mesostasis and microfractures are completely altered to chlorite and/or albite, with accessory amphibole, apatite, pyrite, and chalcopyrite (Figure 4B). In places, clinopyroxene and titanomagnetite rims are altered to chlorite + amphibole. Igneous plagioclase and clinopyroxene grains are extensively intersected by healed microfractures and cleavage planes that contain fluid inclusion suites similar to those described above for RN-19. Epidote veins and quartz + epidote amygdales are uniquely present in TEE intrusions.

TED dolerites (intrusions 3 through 5; Figure 3) contain subeuhedral plagioclase xenocrysts, euhedral olivine phenocrysts, and have finer-grained ophitic and coarser-grained subophitic domains (Figure 4C). Olivine ranges up to 0.3 mm, and accounts for 3–4% of the volume, and while it is completely replaced by chlorite + quartz (and hornblende at increasing depth), olivine pseudomorphs can be distinguished in thin section by the habit and replacement mineral assemblage. The mesostasis contains a similar alteration assemblage to TEE dolerites, although apatite, pyrite, chalcopyrite, and titanite are much finer. Clinopyroxene is altered to chlorite along grain boundaries and is uralitized in more altered zones (Figure 4D). Samples of fine-grained basalt intrusions (intrusions 2 and 6; Figure 3) were not available for whole-rock analysis, but are assumed to have a TED affinity based on a high proportion of olivine phenocrysts typical of TED "picrite" surface basalt flows. Intrusions 2 and 6 consist of fine-grained basalt with chilled margins containing 3–4% of 0.2–0.8 mm olivine grains that have been completely replaced by chlorite + quartz, while hornblende is noticeably absent. The chilled margins were likely glassy intrusion contacts, consistent with the igneous texture and lack of obvious flow banding or vesiculation that would distinguish a lava flow top or bottom. The originally glassy matrix of chilled margins is completely replaced by chlorite. Intrusions 4 and 6 occur in fractured core intervals and are distinguishable based on chilled margins in some of the fractured material.

In thin section, TEE dolerites (intrusions 1A through 1E; Figure 3) are generally coarser-grained than TED dolerites and contain more abundant titanomagnetite. Another important distinction is the lack of healed microfractures with secondary fluid inclusions in TED dolerites. Albitization is more extensive in TEE dolerites along these microfractures (Figure 4B compared to Figure 4D). With one exception, definitive contacts between the TEE and TED dolerites (intrusions 3 through 5; Figure 3) occur in fractured core intervals. In this one location, the TED intrusion quenched against the adjacent TEE intrusion, indicating it is younger.
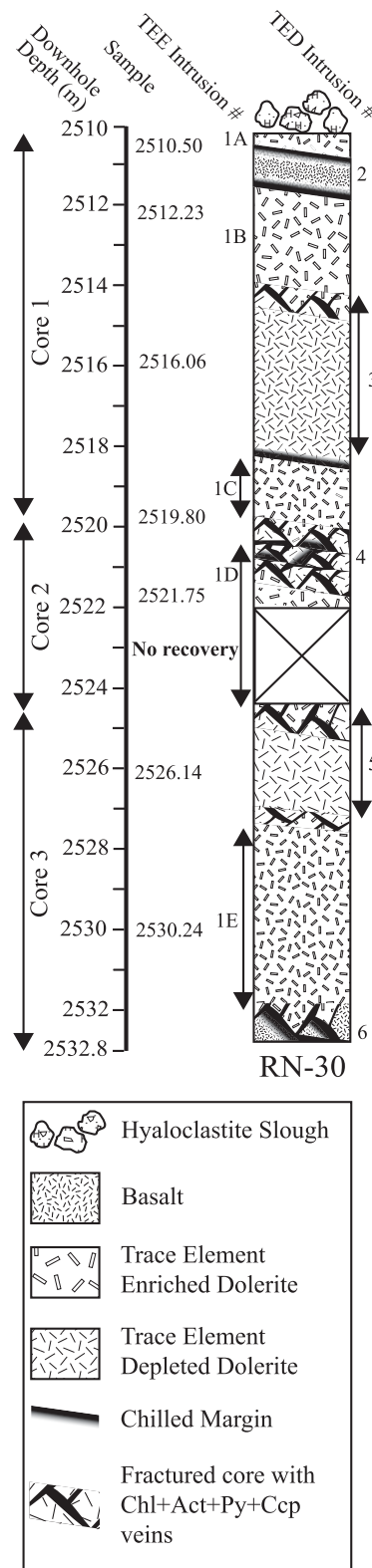
Figure 3. Drill log of the three sequential RN-30 drill cores. RN-30 consists of a series of dolerite and fine-grained basalt intrusions with either a trace element enriched (intrusions 1A through 1E) or trace element depleted igneous affinity (intrusions 3 through 5), verified using whole-rock major and trace element analyses. Fine-grained basalt intrusions 2 and 6 were not analyzed geochemically, but are assumed to belong to the TED group based on the abundance of olivine phenocrysts. A series of hyaloclastite slough blocks were recovered with the core, and come from an unknown depth above.
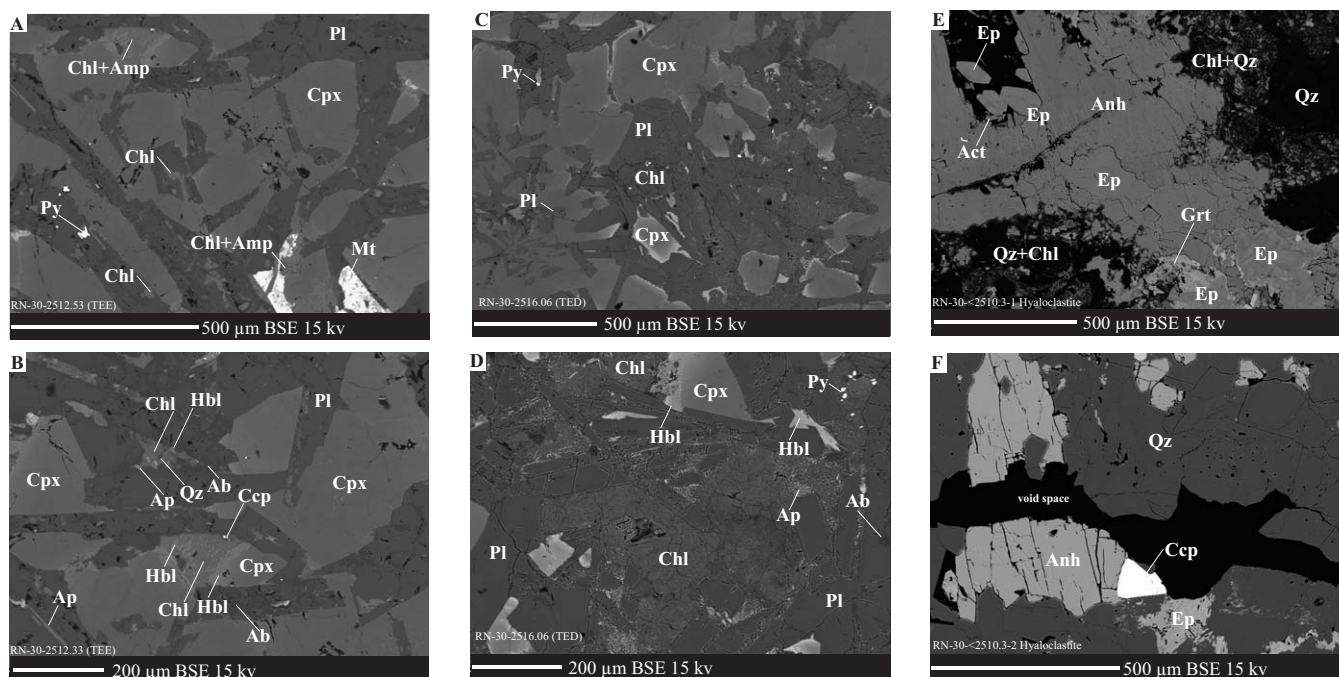
Figure 4. Back scattered electron images of RN-30 samples. (A) Example of TEE dolerite (2512.53 m) igneous texture and (B) alteration of the mesostasis, predominantly to chlorite. (C) Example of TED dolerite (2516.06 m) igneous texture and (D) alteration of the mesostasis, predominantly to chlorite. (E) Several generations of alteration are apparent in hyaloclastite slough blocks (see text for details). Secondary anhydrite and quartz dominate the hyaloclastite slough blocks in veins (E) and in the matrix (F). Act = actinolite, Amp = amphibole, Anh = anhydrite, Ap = apatite, Ccp = chalcopyrite, Chl = chlorite, Cpx = clinopyroxene, Ep = epidote, Grt = garnet, Hbl = hornblende, Mt = titanomagnetite, Ol = olivine, Pl = plagioclase, Prh = prehnite, Py = pyrite, Qz = quartz.

Several hyaloclastite "rollers" were returned as slough on top of the RN-30 core. The slough contains fine-grained basalt fragments that suggest a chilled margin may be present. The hyaloclastite preserves few original textures and records multiple generations of alteration: epidote + actinolite veins followed by garnet + apatite replacing epidote, followed by quartz + chlorite veins, followed by anhydrite veins (Figures 4E and 4F). The hyaloclastite is intersected by 1–10 mm anhydrite + quartz veins. Fe-oxide is present in some of the thinner anhydrite veins. The hyaloclastite cobbles were recovered from an unknown depth above the intrusions, but based on cutting logs and geophysical logs, likely came from ~2450 m depth.

2.2. Analytical Methods

Samples cut from the RN-19, RN-17B, and RN-30 core were selected to avoid large veins and vugs. The outer core edge that was in contact with the drill bit and core barrels was removed using a diamond edge rock saw and rinsed with deionized water to minimize potential trace metal contamination from the drill bit. Samples were selected to avoid secondary mineral veins, but microscopic chlorite/actinolite veins were impossible to avoid in some samples. The extensive network of anhydrite and quartz veins could not be excluded from the RN-30 slough blocks, and space-filling albite was also incorporated in hyaloclastite and lithic breccia samples from the RN-17B core for the same reason. Major, trace element, and loss on ignition (LOI) determinations were performed on bulk rock samples of drill core and drill cuttings at Washington State University (WSU) GeoAnalytical Laboratory. Samples were ground in a tungsten carbide ring mill. Major and trace element concentrations were measured using X-ray fluorescence spectrometry (XRF) and inductively coupled plasma mass spectrometry (ICP-MS). Samples analyzed by XRF were prepared according to the methods outlined in *Johnson et al.* [1999] and analyzed using a Thermo-ARL AdvantXP instrument. Samples analyzed by ICP-MS were prepared according to the methods outlined in *Jenner et al.* [1990] and analyzed using an Agilent 4500 ICP-MS. The limit of determination (LOD) reported for XRF measurements was provided by WSU, and is the 2-sigma limit determined from analyzing 250 repeat measurements made over 14 months (Table 1). The LOD reported for ICP-MS data is derived from the concentration equivalent of the analytical blank + 3 times the standard deviation of the concentration equivalent of replicate

Table 2. REE and Y Concentrations in Hornblende Replacing Glassy Protolith in Samples From the IDDP Core RN-17B[a]

	Y (ppm)	La (ppm)	Ce (ppm)	Pr (ppm)	Nd (ppm)	Sm (ppm)	Eu (ppm)	Gd (ppm)	Tb (ppm)	Dy (ppm)	Ho (ppm)	Er (ppm)	Tm (ppm)	Yb (ppm)	Lu (ppm)
Hyaloclastite Shard															
2798.64 m^{-1}	31	0.22	1.05	0.28	2.11	1.55	0.60	3.52	0.75	5.49	1.24	3.71	0.53	3.31	0.47
2798.64 m^{-2}	31	0.31	1.49	0.39	2.95	2.16	0.63	3.89	0.80	5.81	1.29	3.67	0.52	3.09	0.40
2798.64 m^{-3}	27	0.23	1.09	0.27	1.99	1.48	0.55	2.89	0.65	4.74	1.07	3.23	0.46	2.68	0.34
2798.64 m^{-4}	27	0.14	0.73	0.20	1.57	1.28	0.48	2.71	0.59	4.62	1.04	3.18	0.43	2.79	0.36
Hyaloclastite Shard															
2799.75 m^{-1}	23	0.14	0.62	0.16	1.22	0.99	0.43	2.12	0.49	3.84	0.89	2.68	0.38	2.60	0.34
2799.75 m^{-3}	40	0.39	2.29	0.59	4.14	2.46	0.76	4.30	0.95	6.97	1.48	4.67	0.68	4.78	0.73
2799.75 m^{-4}	36	0.68	3.15	0.70	4.19	2.14	0.66	3.69	0.78	5.85	1.33	4.13	0.64	4.31	0.68
2799.75 m^{-5}	41	0.79	3.67	0.82	4.80	2.43	0.76	4.18	0.88	7.02	1.45	4.60	0.69	4.56	0.64
Gassy Clast Rim															
2802.9 m^{-1}	18	0.03	0.19	0.06	0.60	0.64	0.22	1.53	0.35	2.88	0.66	2.19	0.34	2.68	0.43
2802.9 m^{-2}	24	0.10	0.62	0.20	1.69	1.28	0.47	2.76	0.59	4.67	0.98	2.93	0.42	2.46	0.28
2802.9 m^{-3}	19	0.07	0.36	0.10	0.82	0.70	0.24	1.70	0.36	3.02	0.70	2.21	0.35	2.46	0.42
2802.9 m^{-4}	23	0.07	0.34	0.09	0.84	0.86	0.26	2.02	0.47	3.64	0.89	2.78	0.41	3.12	0.46
2802.9 m^{-5}	21	0.03	0.14	0.04	0.44	0.51	0.19	1.56	0.37	3.00	0.76	2.56	0.39	2.97	0.51
Gassy Clast Rim															
2804.3 m^{-1}	14	0.03	0.25	0.10	0.91	0.74	0.19	1.58	0.34	2.47	0.54	1.76	0.25	1.95	0.32
2804.3 m^{-2}	12	0.02	0.13	0.06	0.60	0.57	0.11	1.16	0.27	2.01	0.45	1.56	0.24	1.98	0.36
2804.3 m^{-3}	16	0.03	0.24	0.09	0.78	0.75	0.13	1.65	0.34	2.82	0.56	1.97	0.32	2.39	0.39
2804.3 m^{-4}	12	0.02	0.12	0.05	0.58	0.56	0.09	1.35	0.27	2.12	0.47	1.57	0.23	1.66	0.30
2804.3 m^{-5}	11	0.02	0.16	0.06	0.65	0.61	0.14	1.13	0.24	1.76	0.43	1.45	0.23	1.80	0.34
% RSD KL2-G (n = 8)	2.6	1.6	2.1	1.8	2.5	3.1	2.3	2.8	2.4	2.6	2.9	2.8	3.5	0.8	5.0
% Error KL2-G	−0.8	0.7	0.6	0.7	−0.4	1.6	0.3	0.5	−0.6	−0.5	0.0	2.0	0.3	−0.1	0.0

[a]Percent relative standard deviation (% RSD) is based on repeated measurements of the MPI-DING KL2-G basalt glass standard. Percent error is the analytical accuracy is reported as the average of the differences between the measured value and the established concentration of each element the MPI-DING KL2-G standard.

measurements of the analytical blank (Table 1). The plots presented in this study utilize the value of the LOD for analytes reported below the respective LOD. We acknowledge that values near the LOD have associated errors approaching ±100%.

Measurements of selected trace elements in hornblende from the RN-17B core were performed on standard polished thin sections using laser ablation inductively couple plasma mass spectrometry (LA-ICP-MS). Analyses included hydrothermal hornblende replacing hyaloclastite shards (2798.64 and 2799.75 m) and glassy rims on clasts in lithic breccia (2802.9 and 2804.3 m). Analyses were performed at UC Davis using an Agilent 7700x quadrupole ICP-MS with an additional rotary exhaust pump connected in-line with the standard pump to lower detection limits and improve precision [*Günther and Hattendorf*, 2005].

The ICP-MS was coupled to a Photon Instruments 193 nm ArF excimer laser equipped with an ANU-style HelEx dual-cell ablation chamber. Material was transported from the ablation cell using helium as a carrier gas, which was subsequently mixed with argon gas prior to introduction into the plasma. Tuning was performed while ablating standard reference material (SRM) NIST 610 to maximize sensitivity, to minimize the ThO^+/Th^+ ratio, and to maintain the U^+/Th^+ intensity approximately equal to the concentration ratio in the standard ($\sim$1). The MPI-DING ML3B-G basalt glass was used as a calibration standard, and the MPI-DING KL2B-G basalt glass was analyzed as an unknown. ^{43}Ca was used for internal element standardization, and the Ca content of hornblende (12.25 wt %) is the average of RN-17B hornblende values measured by electron microbe that were reported by *Fowler et al.* [2015].

The LA-ICP-MS analytical precision is reported as the percent relative standard deviation (% RSD) of repeated measurements of the SRMs, and analytical accuracy is reported as the average of the differences between the measured value and the established concentration of each element monitored in the SRMs reported in percent. Accuracy is within 2.7% and precision is within 5.9% (Table 2). Data were reduced using Iolite software [*Paton et al.*, 2011], incorporating values for the MPI-DING standards from *Jochum et al.* [2006]. The detection limit (essentially 3σ * background measured before and after each laser spot analysis) was calculated using the equation of *Longerich et al.* [1996], which is incorporated in the Iolite software data reduction scheme.

3. Results

3.1. Whole-Rock and LA-ICP-MS Analytical Results

Whole-rock analytical results for drill core samples are provided in Table 1. Whole-rock results for refractory elements in the Reykjanes drill cores that are generally considered immobile during hydrothermal alteration are presented on chondrite normalized [*McDonough and Sun*, 1995] spider diagrams (Figures 5A and 5B); included for reference is the range of values for TEE and TED unaltered surface basalts compiled from published sources [*Revillon et al.*, 1999; *Skovgaard et al.*, 2001; *Kokfelt*, 2006; *Koornneef et al.*, 2012]. Results are also plotted in terms of immobile element ratios (Nb/Zr and Y/Zr) which differentiate unaltered TEE and TED surface basalts (Figure 5C). Unaltered TEE surface basalts plot at Y/Zr ratios <0.38, and unaltered surface TED basalts plot at Y/Zr values >0.58 (Figure 5C).

The RN-19 and RN-30 dolerite samples have relatively low LOI (<1.0–1.6 wt %), while RN-30 hyaloclastite and RN-17B rocks have higher LOI (up to 4.88 wt %) that correspond to higher proportions of hydrous alteration minerals. For comparison, LOI in whole-rock samples of the sheeted dike sections of Holes 504B and 1256D range 0–6.0 and 0–4.7%, respectively [*Kurnosov et al.*, 2008; *Huang et al.*, 2015]. Despite clear evidence that all samples in this study are altered to some degree, the alteration characteristics have not obscured the magmatic affinity to unaltered TED and TEE surface basalts recorded by immobile element concentrations (Figures 5A and 5B) or ratios (Figure 5C). In contrast, isotope ratios ($^{87}Sr/^{86}Sr$, $^{143}Nd/^{144}Nd$, and $^{206}Pb/^{204}Pb$) are not a definitive measure of the magmatic affinity (e.g., TEE or TED protolith) of Reykjanes basalts due to overlap of isotope values between the two groups (Figure 6). The isotopic variations are useful for identifying mantle heterogeneities, but they cannot be used to distinguish the compositional protoliths (e.g., TEE or TED) of the altered rocks for the purpose of constraining the chemical exchange between the basalts and hydrothermal fluids, as discussed below. It has also been suggested that these isotope systems may be modified during seawater-basalt interaction [*Verma*, 1992].

An important consideration is that analytical error approaches ±100% for element concentrations that approach the LOD. This is particularly important for K, Rb, and Pb in TEE rocks, which are reported at levels near the LOD (Table 1). The average concentration of K_2O in unaltered TEE surface rocks is 0.2 wt % (references in Figure 5 legend) compared to the LOD reported in this study of 0.031 wt % (LOD) for K_2O. Rb values are 3.5 ppm (unaltered) compared to 0.057 ppm (LOD), and Pb values are 0.53 ppm (unaltered) compared to 0.204 (LOD). The average value of K, Rb, and Pb in unaltered TEE rocks, the assumed protolith, is much greater than 100% of the LOD value, so there is a sufficient level of confidence in the results to infer hydrothermal mobilization of these elements even considering large relative errors for values near the LOD.

3.2. LA-ICP-MS Results for REE in Hornblende

LA-ICP-MS results for hornblende replacing hyaloclastite shards and originally glassy pillow and breccia clast margins in the RN-17B core are provided in Table 2. An attempt was made to measure Y and the rare earth elements (La through Lu) in space-filling hydrothermal albite from RN-17B using LA-ICP-MS; however, the results were statistically indistinguishable from background and thus are not included in analytical tables. All hornblende samples are LREE (La through Eu) depleted with negative EU anomalies compared to the adjacent whole-rock samples, while HREE (Gd through Lu) values for hornblende are within error of adjacent whole-rock samples (Figure 7). The results show that while HREE are relatively immobile in glassy protolith material that is completely altered to hornblende, there are large losses of LREE relative to the chlorite-dominated crystalline clasts that dominate the samples submitted for whole-rock chemistry.

3.3. Determination of Protolith and Elemental Gains and Losses

Element concentrations in primary rocks are "diluted" by secondary open-space filling mineralization, and modified by alteration-induced density changes during the formation of hydrous alteration minerals [e.g., *Gresens*, 1967; *Barrett and MacLean*, 1994; *Grant*, 1986; *Franzson et al.*, 2008]. Scaling concentrations to a hydrothermally immobile element is useful for removing the effects of dilution and density changes in order to gauge concentration changes of highly mobile elements. This method was used to calculate hydrothermal fluxes of elements recorded by samples from Hole 504B by scaling highly mobile elements to Nb [*Bach et al.*, 2003]. Despite some degree of alteration for all of the Reykjanes drill core samples, the TEE or
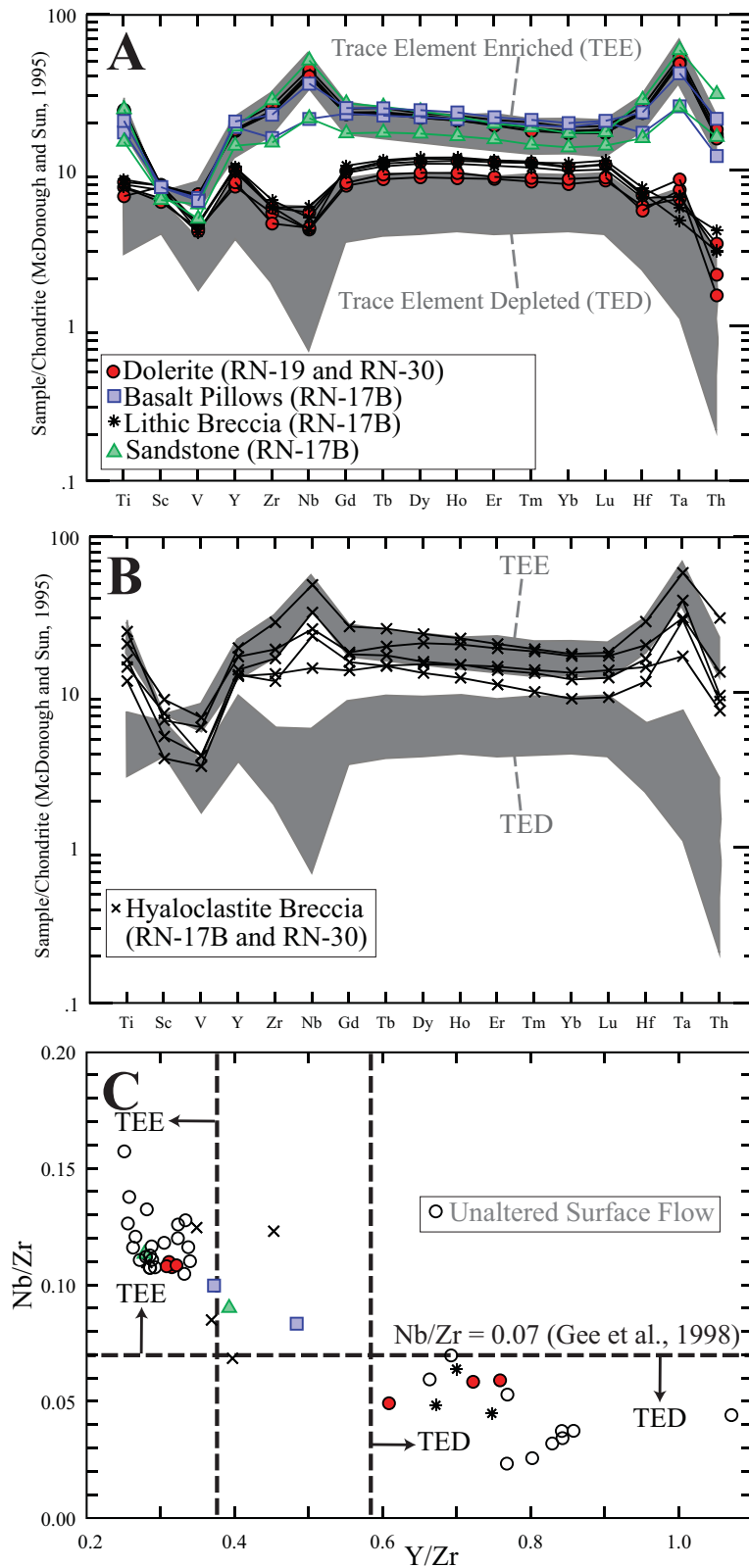
Figure 5. (A, B) Chondrite-normalized [*McDonough and Sun*, 1995] spider diagrams of refractory elements in whole-rock samples from RN-17B, RN-19, and RN-30 drill cores. (B) Hyaloclastite samples are broken out for clarity. Shaded regions indicate the range of values for unaltered surface flows. (C) Sample protolith affinities are distinguishable in terms of Nb or Y normalized to Zr. Values for unaltered surface samples from *Gurenko and Chaussidon* [1995], *Revillon et al.* [1999], *Chauvel and Hemond* [2000], *Skovgaard et al.* [2001], *Kokfelt* [2006], *Brandon et al.* [2007], *Nielson et al.* [2007], *Peate et al.* [2009], and *Koornneef et al.* [2012].
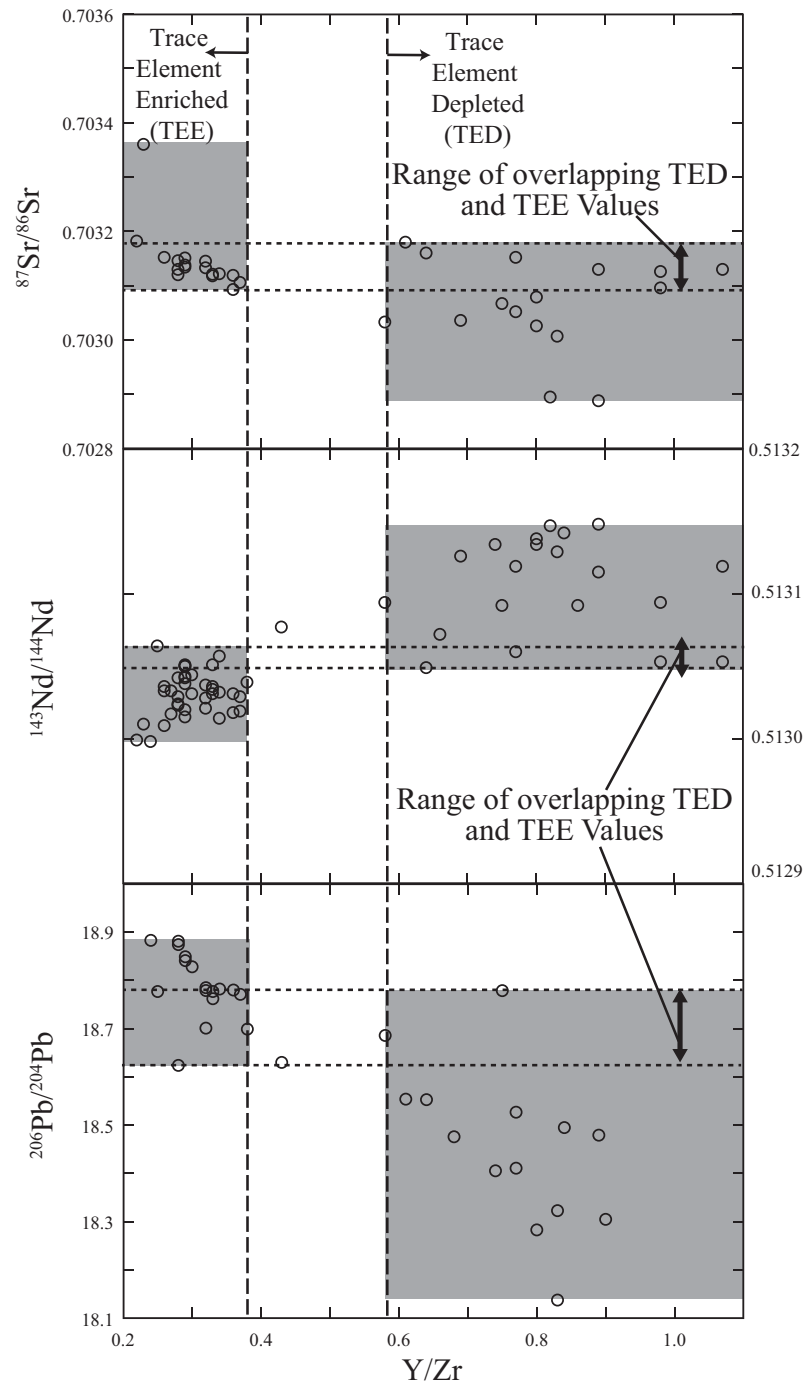
Figure 6. Range of literature values for isotope systems ($^{87}Sr/^{86}Sr$, $^{143}Nd/^{144}Nd$, $^{206}Pb/^{204}Pb$) measured in unaltered surface basalt flows on the Reykjanes Peninsula compared to the Y/Zr ratio. The suggested overlap in the plotted isotope systems is a minimum estimate, as analytical error is not considered in the plot. Values from *Zindler et al.* [1979], *Elliott et al.* [1991], *Hemond et al.* [1993], *Gee et al.* [1998], *Revillon et al.* [1999], *Chauvel and Hémond* [2000], *Kempton et al.* [2000], *Skovgaard et al.* [2001], *Thirlwall et al.* [2004], *Kokfelt* [2006], *Brandon et al.* [2007], *Nielsen et al.* [2007], *Peate et al.* [2009], *Martin and Sigmarsson* [2010], and *Koornneef et al.* [2012].

TED affinity is not obscured when a suitable immobile element is selected as an alteration monitor (Figure 5C).

Subaerially erupted, unaltered TEE and TED basalts on the Reykjanes Peninsula are readily distinguished based on the ratios of a range of refractory trace elements, and typically the Nb/Zr ratio is used [*Gee et al.*,
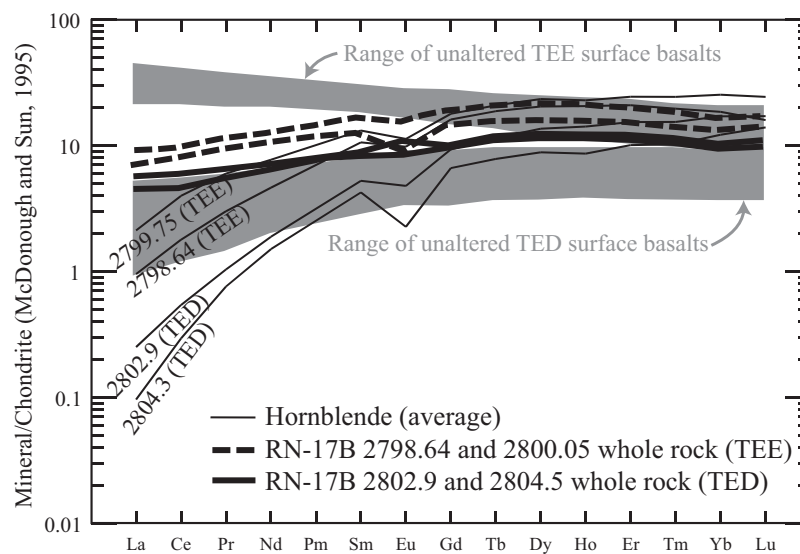
Figure 7. Rare earth element concentrations in hydrothermal hornblende entirely replacing pillow basalt rinds and hyaloclastite shards in the RN-17B core. REE were measured using LA-ICP-MS. The average hornblende value from Table 2 is plotted for each depth interval. The REE content of adjacent whole-rock samples and unaltered surface basalts is included for comparison (see references in Figure 5 legend for data sources).

1998; *Peate et al.*, 2009] (Figure 2). While Nb is generally considered immobile during alteration, grinding of samples in a tungsten carbide ring mill has the potential to contaminate samples with Nb and Ta [*Joron et al.*, 1980; *Jochum et al.*, 1990]. Because samples were ground in a tungsten carbide ring mill for this study, we instead use the Y/Zr ratio to distinguish a TEE or TED protolith affinity (Figures 5C and 8). In cases of extreme alteration, it challenging to identify any suitable alteration monitor. Four samples from the RN-17B core fall between Y/Zr values of 0.38 and 0.58 suggesting a unique protolith or mixed affinity (Figure 5C), while refractory element characteristics of the four samples are similar to TEE rocks (Figures 5A and 5B). The four samples show strong indications of REE gains relative to the assumed protolith (Figure 8), suggesting Y may also have been gained in these samples based on chemical similarity of Y to the REE. Y gain relative to the protolith would shift samples from TEE Y/Zr values toward TED Y/Zr values. The altered samples that plot between Y/Zr values of 0.38 and 0.58 are treated as having a TEE protolith.

In order to gauge the direction of elemental changes (gains or losses), we normalized samples to Zr (Figure 8), which is generally immobile even during high degrees of hydrothermal alteration [*Humphris and Thompson*, 1978b; *Floyd and Winchester*, 1978; *Zierenberg et al.*, 1988; *Barrett and MacLean*, 1994; *Franzson et al.*, 2008]. Aside from low susceptibility for mobilization by hydrothermal processes, Zr is a particularly good alteration monitor because it is present at fairly high concentrations relative to other trace elements. The generally high concentrations minimize error in analytical measurement and compensate for any slight mobilization or sample inhomogeneity.

4. Discussion

Alteration and elemental gains and losses are distinct for RN-30 dolerite compared to the extrusive RN-17B rocks and RN-30 hyaloclastite slough blocks that were originally emplaced in contact with cold seawater on the seafloor. We use the term "extrusive" to refer to rocks originally emplaced on the seafloor that include hyaloclastite, lithic breccia, basalt sandstone, and basalt pillow formations. Rocks originally emplaced on the seafloor are present at the current depths owing to down faulting and burial by continued volcanism [*Björnsson et al.*, 1972; *Friðleifsson and Richter*, 2010; *Fowler et al.*, 2015]. In contrast, grain size, ophitic textures, and chilled margins in RN-30 and RN-19 TEE and TED dolerites indicate subsurface intrusion. In addition to the mode of emplacement, the crystallinity of intrusive and extrusive rocks differs as does the nature and extent of alteration. Intrusive rocks are largely coarse-grained, while the extrusive rocks contain finely crystalline protolith and glass in hyaloclastite shards and pillow basalt rims. In the RN-30 and RN-19 intrusive TEE and TED dolerite, alteration is dominated by chlorite and is largely restricted to mesostasis and grain
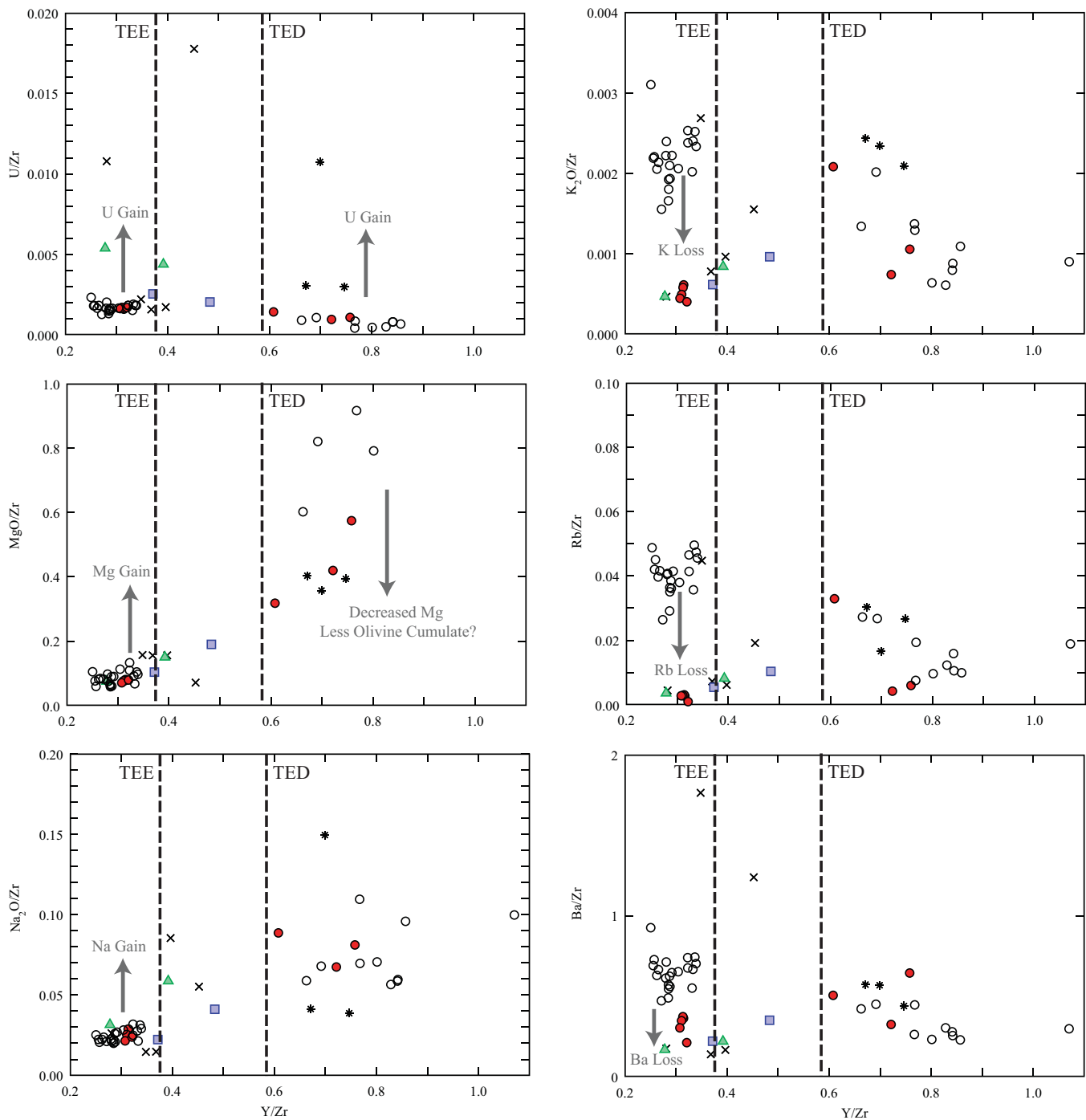
Figure 8. Comparison of Zr-normalized concentrations for elements and oxides in altered Reykjanes drill core samples and unaltered equivalents (open circles). Data points with values below the respective LOD are plotted at the value of the LOD. The error of values at or approaching the LOD are ±100% (e.g., Cu, Pb, and Rb). Data source and legend same as for Figure 5.

edges. In the RN-17B extrusive rocks, glass and small crystalline clasts are almost entirely altered to hornblende and calcic plagioclase, while fine-grained interiors of crystalline clasts largely contain chlorite. In the RN-30 hyaloclastite slough blocks, alteration of primary material is dominated by chlorite, actinolite, and epidote. The following discussion of hydrothermal element gains and losses assumes that rocks in the studied drill core samples had protolith compositions similar to surface basalt flows at Reykjanes prior to alteration. While Figure 5 suggests this is the case for several refractory elements along with Nb/Zr and Y/Zr ratios, this assumption is extended to a range of major and trace elements.
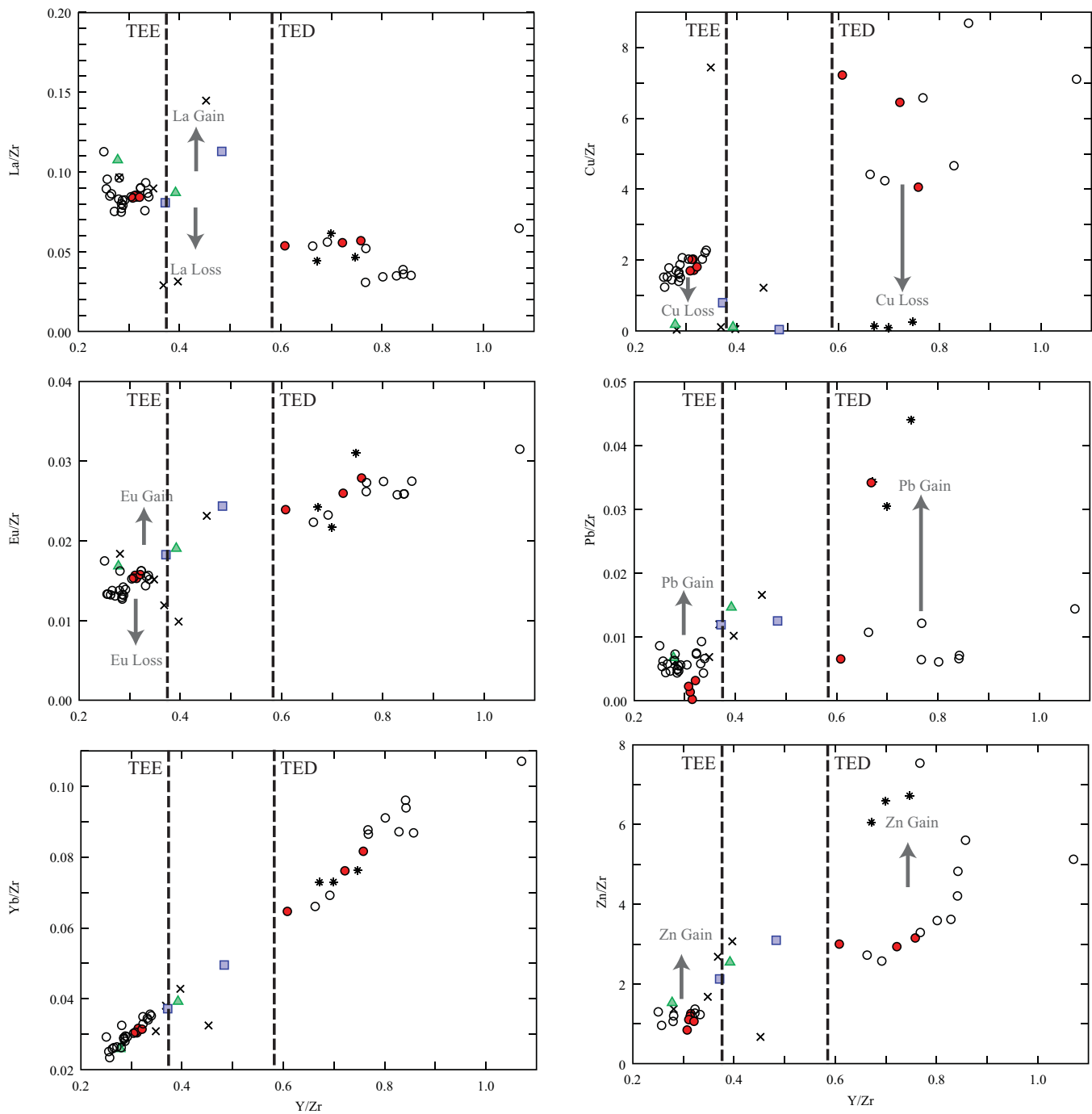
Figure 8. (Continued).

4.1. Rocks With a TED Affinity

The compositional heterogeneity of rocks with a TED protolith, which includes lithic breccia samples from the RN-17B core and dolerite samples from the RN-19 and RN-30 cores, presents a challenge for distinguishing hydrothermal gains and losses of elements. The compositional heterogeneity of TED rocks results from the influence of variable amounts of cumulate phases such as olivine, plagioclase, and titanomagnetite [*Gee et al.*, 1998] that act to "dilute" trace element concentrations. The trace element composition of the TED group is further modified by the trace element characteristics of the diluting cumulate phase. The influence

of cumulate olivine, magnetite/ilmenite, and plagioclase on TED rock compositions is apparent in concentration plots of MgO, Cr, and Al_2O_3 (Figure 9). Obvious gains or losses of elements are not apparent in altered samples with a TED affinity due to the large variability of unaltered equivalents exposed on the Reykjanes Peninsula (Figure 8). The exception is for TED lithic breccia samples from the RN-17B core, which have clear U and Pb gains and Cu loss, similar to elemental changes in adjacent RN-17B rocks with a TEE protolith affinity (Figure 8). Contrary to what the chlorite mesostasis alteration and presence of chlorite and actinolite mineralized fractures would suggest, many TED samples from the three cores appear to have lost Mg relative to the unaltered TED surface basalts (Figure 8). However, this apparent Mg loss potentially reflects a lower proportion of cumulate olivine compared to unaltered surface equivalents (Figure 9).

4.2. RN-30 TEE Dolerites

RN-30 TEE dolerites have lost K, Rb, Ba, and Pb (Figures 8 and 10). Experiments have demonstrated that K, Rb, Cs, and Ba are released from basalt at temperatures above 150°C during reaction with seawater [*Seyfried and Bischoff*, 1979; *Seyfried*, 1987], and Pb is readily mobilized from basalt under hydrothermal conditions [*Chen et al.*, 1986; *Verma*, 1992]. K, Rb, Ba, and Pb were likely hosted in igneous mesostasis, which has been completely replaced by hydrous alteration phases (Figures 4C and 4D). Primary plagioclase, clinopyroxene, and most titanomagnetite remain largely intact (Figures 4A and 4B) and are unlikely the primary source of these elements. While the whole-rock data indicate that RN-30 TEE dolerites have not gained or lost Cu (Figure 8), Cu has likely been gained based on the localized presence of chalcopyrite + pyrite + chlorite on fracture surfaces that were excluded from the whole-rock analysis. This would indicate that the RN-30 TEE dolerites are overall a sink for Cu and Mg, and are not a significant source of these elements.

4.3. Alteration and Elemental Changes in TEE Extrusive Rocks

Element gains and losses in the RN-17B and RN-30 TEE extrusive rock samples are more complex than for the RN-30 TEE dolerite intrusions. Gains of Mg, Na, U, Pb, Zn, and losses of K, Rb, Ba, Sr, and Cu are observed (Figures 8 and 10). Because these rocks were originally emplaced on the seafloor, we examine element gains and losses in the context of subseafloor hydrothermal processes.

The elements U and Mg along with K, Rb, Cs, and Ba are gained by basalt from seawater during weathering and low-temperature diffuse seawater flow through permeable pillow basalt, hyaloclastite, and sediment deposits in hydrothermal recharge zones in the upper oceanic crust [*Hart*, 1969; *Thompson*, 1973; *Humphris and Thompson*, 1978a, 1978b; *Staudigel et al.*, 1981a, 1981b; *Hart and Staudigel*, 1982; *Staudigel and Hart*, 1983; *Chen et al.*, 1986; *Staudigel et al.*, 1996; *Alt*, 1995; *Alt et al.*, 1996; *Teagle et al.*, 1996; *Bach et al.*, 2001, 2003]. The main phases hosting K, Rb, and Cs in the upper oceanic crust are palagonite, nontronite, and celadonite and, at increasing temperature other smectites [*Staudigel et al.*, 1981a; *Hart and Staudigel*, 1982; *Alt*, 1995]. U mobility is controlled by a fluid redox change as initially oxidized seawater is buffered to reducing conditions during reaction with basalt. The result is that uranium is fixed in the crust at less than 80°C by the reduction of seawater U(VI)–U(IV). Uranium is thought to be hosted in Fe-oxides [*Hart and Staudigel*, 1982; *Chen et al.*, 1986; *Alt*, 1995; *Bach et al.*, 2001] formed by the oxidation of ferrous iron in the basalt. Addition of seawater-derived Mg to oceanic crust persists at more elevated temperatures than U and alkali elements [*Bischoff and Dickson*, 1975; *Hajash*, 1975; *Bloch and Hoffman*, 1978; *Humphris and Thompson*, 1978a; *Edmond et al.*, 1979; *Alt*, 1995]. The host phases for Mg are smectite clays at temperatures <200°C and chlorite at temperatures >200°C [*Alt*, 1995].

Assuming U and Mg enrichments in the Reykjanes extrusive rocks result from low-temperature weathering by seawater, we would expect accompanying enrichment of alkali elements (K, Rb, Cs) and Ba; however, these elements have been lost (Figures 8 and 10). Alkali and Ba uptake by oceanic crust from seawater probably ceases at the thermally controlled transition of smectite to chlorite, which occurs at temperatures >200°C in seafloor hydrothermal systems [*Alt*, 1995]. At similar temperatures in the Reykjanes geothermal system, alkali mobilization is facilitated by the temperature-dependent breakdown of the low-temperature clay minerals while Mg continues to be incorporated into chlorite [*Tomasson and Kristannsdottir*, 1972]. We suggest that alkalis were originally gained by the RN-17B and RN-30 extrusive rocks, and remobilized during transition to an elevated hydrothermal temperature regime that facilitated the breakdown of smectite clays. Mg gains persisted at these elevated temperatures due to the formation of chlorite, which is the dominant alteration phase in the extrusive rocks. U was potentially originally hosted by Fe-oxides; however, it is unclear what the hosting phase is now. The reducing conditions that characterize deep fluids in the
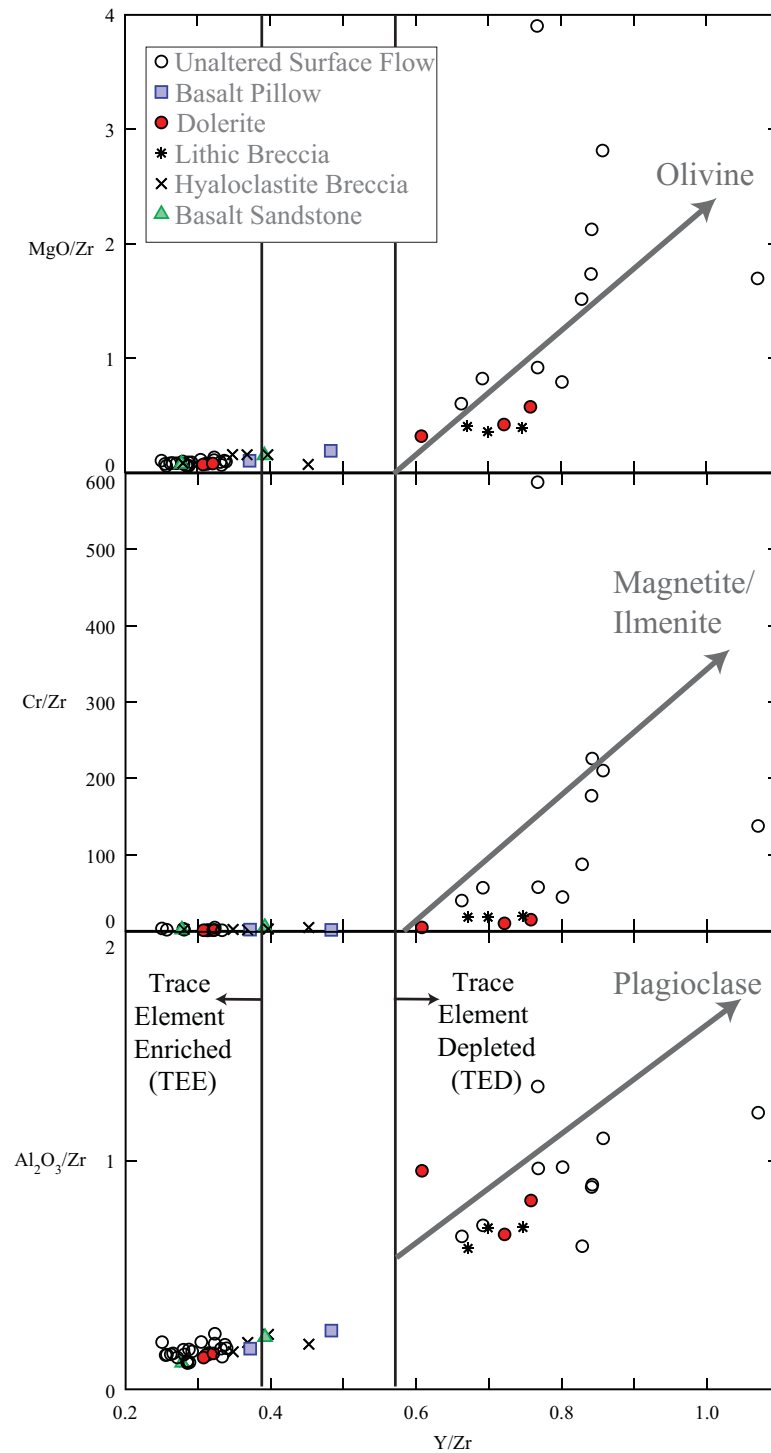
Figure 9. Comparison of Zr-normalized MgO, Cr, and Al_2O_3 for unaltered TEE and TED basalts on the Reykjanes Peninsula (open circles). Whole-rock data for Reykjanes drill core samples are included for comparison (see legend in Figure 5). While the TEE basalts form a distinct cluster, TED basalts have highly variable compositions due to incorporation of variable degrees of cumulate phases. Data sources and legend are same as for Figure 5.

Reykjanes geothermal system [*Stefánsson and Arnórsson*, 2002] likely hinder U remobilization, as U mobilization is widely recognized as requiring oxidizing conditions. Sr loss and Na gain in RN-17B extrusive rocks corresponds with near complete alteration of primary plagioclase to coexisting albite and anorthite, and the common occurrence of albite as a space-filling secondary mineral [*Fowler et al.*, 2015]. The most
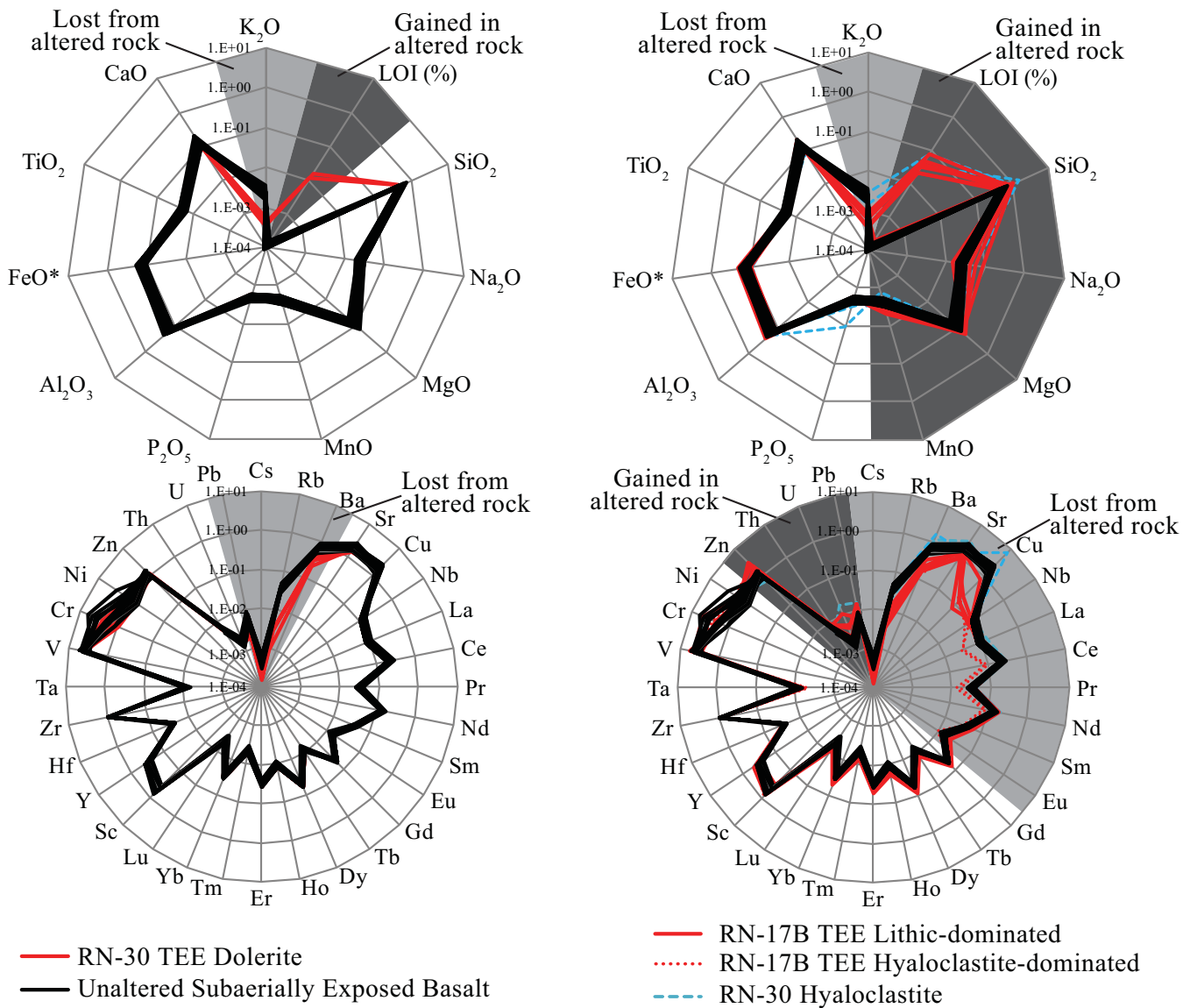
Figure 10. Radar plot of Zr-normalized whole-rock concentrations for RN-30 TEE intrusive dolerite samples (left), and RN-17B and RN-30 TEE extrusive samples (right). Hyaloclastite samples from RN-17B (2798.64 and 2800.05 m) that show significant LREE loss (red line, short dash), and RN-30 hyaloclastite samples (blue line, long dash) are indicated. Altered samples compared to a compilation of 35 values for unaltered, subaerially exposed basalts with a TEE affinity. Major elements are in weight percent (upper) and minor elements in ppm (lower), both upper and lower diagrams are plotted on a logarithmic scale. Where values of altered rocks (red) do not appear, they are within the range of values for subaerially exposed rocks (black). Elements that fall below the LOD are plotted at a value equivalent to the detection limit.

extensively recrystallized rocks in the lower sheeted dike sections from in situ oceanic crust also indicate uptake of Na by albite formation. Recrystallization of plagioclase, which hosts Sr in the Ca crystal site, provides a mechanism to release Sr.

RN-30 hyaloclastite and RN-17B TEE lithologies have lost Cu and gained Pb and Zn (Figures 8 and 10). Apparent Cu gains in one RN-30 hyaloclastite sample is due to vein material that contains chalcopyrite (Figure 4D). Cu concentrations fall below the detection limit in most of the RN-17B extrusive samples (Table 1). Seawater-basalt reaction experiments demonstrate that Cu and Zn are readily mobilized from basalt at low water-rock ratio (1:1) when temperatures exceed 350°C [*Seewald and Seyfried*, 1990]. Cu leaching at lower temperatures requires sustained low pH that is maintained by Mg metasomatism resulting from seawater-

rock interaction at high (>10 to >50) water-rock ratios [*Seyfried and Bischoff*, 1981; *Seyfried and Mottl*, 1982; *Mottl*, 1983; *Reed*, 1983].

Ubiquitous Zn and Pb enrichment and Cu depletion in the RN-17B samples appears to record at least a two-stage alteration history. Fluid inclusion measurements and the occurrence of secondary hornblende and calcic plagioclase in the RN-17B core suggest temperatures exceeded 400°C at some stage in the past [*Fowler et al.*, 2015], which would be more than sufficient to leach Cu, Zn, and Pb. It is however difficult to reconcile near complete loss of Cu in RN-17B rocks without accompanying losses of Pb and Zn. One possibility is that Pb and Zn were introduced as contamination during the drilling processes due to contact of the samples with the drill bit, or precipitated from hot brine due to chilling by cold drilling fluids. While these contamination mechanisms cannot be definitively ruled out, they are unlikely. The outer edge of the 4 inch (∼10 cm) diameter drill cores was removed prior to powdering, and drill bit contamination of the core interiors is unlikely. Pb (0.12–0.29 ppm) and Zn (5–27 ppm) in Reykjanes downhole fluids [*Hardardottir et al.*, 2009] are over an order of magnitude lower than RN-17B whole-rock Pb (0.5–0.98 ppm) and Zn (140–184 ppm). Considering the low primary porosity of the drill core samples, a large flux of hot brine through the samples during drilling would be required to produce the observed Pb and Zn enrichments, which is unlikely considering the hole was fluxed by fresh, cold water during drilling.

We suggest that Zn and Pb in RN-17B extrusive rocks were not sourced from contamination by drilling, but were reenriched at a later stage of hydrothermal activity and fixed in Zn and Pb sulfides precipitated from upwelling fluid, along with the pyrite that is ubiquitous in these rocks. Pyrite, chalcopyrite, and sphalerite are present as secondary sulfide minerals throughout the Reykjanes reservoir rocks [*Libbey and Williams-Jones*, 2016]. Hydrothermal fluids are currently forming high-grade Zn ± Pb sulfide scale in surface pipes at Reykjanes [*Hardardóttir et al.*, 2009]. Scale collected from wells in downhole boiling zones is enriched in Cu, Zn, and precious metals [*Hardardóttir et al.*, 2012] indicating that Zn and Pb gains result from lower temperature mineralization, and readily form in this system.

4.3.1. Rare Earth Elements

LREE are immobile in the majority of the RN-17B and RN-30 TEE extrusive rock samples (Figure 10). LREE loss is observed in two RN-17B hyaloclastite samples from 2798.64 and 2800.05 m (Figure 8) and LREE gains are observed in one RN-30 hyaloclastite sample (<2510.5-1) and one RN-17B pillow basalt sample from 2800.35 m (Figure 8).

REE mobility depends in part on the relative amounts of glass and crystals in the protolith, which affects the accessibility of REE to reaction processes [*Humphris et al.*, 1978]. Leaching experiments on dolerite from Hole 504B showed preferential mobilization of LREE relative to HREE from more reactive interstitial glass than primary igneous minerals [*Bach and Irber*, 1998]. Basalt-seawater experiments and reaction calculations have demonstrated that a high water-rock ratio (>50) is required to maintain low pH during basalt-seawater reactions [*Mottl*, 1983; *Reed*, 1983]. At these high water-rock ratios, significant seawater Mg is taken up by glassy pillow margins, which become totally recrystallized to chlorite [*Alt*, 1995]. REE mobilization from basalt is facilitated by high water-rock ratios [*Ludden and Thompson*, 1979], because REE leaching is significantly more effective in low pH fluids [*Michard*, 1989]. Elevated temperatures are important for REE mobilization and transport also. Hydrothermal and geothermal fluids with temperatures >230°C typically have elevated REE relative to cooler fluids [*Michard*, 1989]. Experimental work showed that Eu decouples from other REE at temperatures greater than 250°C due to a transition from Eu^{3+} to Eu^{2+} under reducing conditions typical of hydrothermal systems, while the other REE remain in a trivalent state [*Sverjensky*, 1994]. LREE chloride complexes (particularly La^{3+} and Eu^{2+}) are increasingly stable in chloride-rich fluids at temperatures >250°C, and in part contribute to the distinctive chondrite normalized pattern of hydrothermal vent fluids that are LREE-enriched with a positive Eu anomaly [*Allen and Seyfried*, 2005; *Migdisov et al.*, 2009]. In summary, significant REE mobilization occurs above 200°C and at high water-rock ratios, conditions where chlorite rather than lower temperature clay minerals are stable [*Alt*, 1995]. In contrast, REE gains are typical of oxidative weathering of rocks on the seafloor and are often accompanied by gains of U, Mg, K, Rb, Cs, and Ba, although gains can occur at higher temperatures owing to destabilization of aqueous REE Cl-complexes during cooling of hot hydrothermal fluids.

We attempted to measure the REE content of space-filling albite using LA-ICP-MS to determine whether that space-filling albite in whole-rock samples could be responsible for the apparent REE loss in RN-17B

hyaloclastite samples 2798.64 and 2800.05 by diluting the whole-rock sample. The albite REE content was well below detection, so while the incorporation of any albite could reduce the overall REE content by diluting whole-rock samples, it would not significantly modify relative LREE and HREE ratios. RN-17B samples showing LREE loss contain a higher proportion of glassy protolith material altered to hornblende compared to other RN-17B rocks that contain relatively more crystalline protolith material dominated by chlorite alteration [*Fowler et al.*, 2015]. We measured the REE content of hornblende replacing hyaloclastite shards and clast margins to test whether that the abundance of glassy lithologies altered to hornblende might control apparent whole-rock REE loss. In all cases, hornblende is significantly LREE-depleted and has a negative Eu anomaly compared to any RN-17B whole-rock REE value, which assumedly approximates the original REE values of the glassy material (Figure 7).

One possibility is that REE were lost from more reactive material during a period of elevated temperatures that facilitated enhanced LREE transport as aqueous chloride complexes. The hornblende in Reykjanes rocks formed at temperatures in excess of 400°C [*Marks et al.*, 2010, 2011]. In the case of the RN-17B core, this likely occurred due to proximal intrusion of a dike followed by cooling to the current in situ temperature of 345°C [*Fowler et al.*, 2015]. Similar (although not as extreme) LREE losses and development of a negative Eu anomaly have been documented for a pillow basalt margin recrystallized to chlorite at the pillow basalt—sheeted dike transition zone in Hole 504B [*Alt and Emmerman*, 1985]. Similar to RN-17B, rocks in the Hole 504B transition zone experienced a temperature spike to 380°C prior to cooling back to 200°C [*Alt et al.*, 1985]. Also similar to the two crystalline RN-17B rocks that have gained LREE and have positive Eu anomalies, many crystalline pillow basalt and upper sheeted dike samples from Hole 504B have gained LREE and have positive Eu anomalies [*Alt and Emmerman*, 1985].

LREE were not necessarily lost during a temperature spike and conditions that resulted in hornblende crystallization. LREE loss potentially occurred at lower temperatures prior to hornblende formation owing to high fluid throughflow in the originally porous hyaloclastite and along pillow and clast margins, which maintained low pH fluids with the potential to leach REE from the reactive glass protolith. Less porous crystalline clast interiors likely experienced lower effective water-rock ratios that were less effective at leaching LREE and in some cases facilitated net LREE deposition. Variable initial porosity and fluid flow through in portions of the RN-17B core could explain why LREE are gained or lost in rocks that experienced similar temperature extremes but are dominated by different alteration assemblages. If high fluid flow through resulted in LREE loss, alteration still likely occurred at temperatures in excess of 250°C, which would promote enhanced LREE fractionation through the formation of aqueous chloride complexes. While it is possible that coexisting LREE gains and losses reflect variable effective water-rock ratios at elevated temperatures, it cannot be ruled out that LREE gains in the RN-30 hyaloclastite and RN-17B pillow basalt samples reflect the initial low-temperature oxidative weathering by seawater that also resulted in U gains.

4.4. Comparison of Reykjanes Rocks With Samples of Altered Oceanic Crust
4.4.1. U and Mg

Progressive depletion of Mg and U from seawater and addition to the oceanic crust along a hydrothermal recharge path results in nearly total absence of these elements in venting hydrothermal fluids [*Chen et al.*, 1986; *Alt*, 1995]. The result is a U and Mg-depleted fluid that continues to react with oceanic crust [*Chen et al.*, 1986; *Alt*, 1995]. This model is consistent with observations from ODP/IODP Hole 1256D [*Teagle et al.*, 2006; *Wilson et al.*, 2006; *Alt et al.*, 2010] and DSDP/ODP Hole 504B [*Alt et al.*, 1986; *Bach et al.*, 2003]. While the upper volcanic sections in 1256D and 504B are enriched in Mg and U, there are no significant Mg or U gains in rocks from the sheeted dike section of these holes during the on-axis phase of alteration [*Alt et al.*, 1996; *Bach et al.*, 2001, 2003].

Low-temperature weathering by seawater of Reykjanes rocks originally emplaced on the seafloor is reflected by both U and Mg gains in RN-17B and RN-30 extrusive rocks. At the in situ temperature where the RN-17B core was recovered, Mg is hosted in metastable chlorite, which is altering to amphibole, and low-temperature clay minerals are not preserved [*Fowler et al.*, 2015]. RN-30 TEE dolerites do not record apparent gains in Mg and U despite the nearly complete alteration of mesostasis to chlorite, suggesting they have only ever interacted with an upwelling fluid already depleted in Mg and U.

4.4.2. K, Rb, and Ba

Alkali losses in the RN-30 TEE dolerites and RN-17B extrusive rocks are comparable to the upper and lower sheeted dike sections in DSDP/ODP Hole 504B that are leached of K and Cs [*Alt et al.*, 1996; *Bach et al.*, 2003]. At Pito Deep on the NE edge of the Easter microplate, the upper sheeted dikes exposed on a submarine scarp have gained K and Rb and show little mobility of other major elements, while the lower sheeted dike section has lost K and Rb [*Heft et al.*, 2008]. The alkali losses and lack of Mg or U gains in the RN-30 TEE dolerites is consistent with alteration by a Mg-depleted fluid at depth, as hypothesized by *Alt et al.* [1996] for the sheeted dike section in Hole 504B. Importantly, the RN-30 TEE dolerites were recovered from active hydrothermal conditions and have unlikely been exposed to low-temperature weathering or alteration that potentially reenriches alkalis to some degree in dolerite samples recovered from in situ oceanic crust.

Compared to drill core samples of in situ ocean crust that experienced alteration at extreme ($>400°C$) temperatures, the abundance of clastic (breccia, hyaloclastite, and volcanic sand) lithologies recovered in the RN-17B core is somewhat unusual. However, the clastic rocks all suggest local transport and deposition near the eruptive center. We note that the core recovery in RN-17B was near 100%, whereas recovery of rocks from upper oceanic crust drilled at sea are typically low, and may be biased due to selective recovery of more competent lithologies, particularly basalt flows. Despite the unusual abundance of clastic rocks in RN-17B, it is clear that RN-17B rocks were derived from basaltic eruptions on the seafloor, typical of numerous volcanic sections of upper oceanic crust that have undergone background weathering and low-temperature hydrothermal alteration [e.g., *Alt*, 1995]. Coexisting U and Mg gains in the RN-17B TEE extrusive rocks are typical of low-temperature alteration in numerous examples of the upper volcanic section recovered from the seafloor and upper levels of in situ oceanic crust. However, the alkali and Ba losses are somewhat unique. It is difficult to explain the U and Mg gains without associated alkali gains, suggesting alkali elements were remobilized. The persistence of the interpreted early Mg and U gains at elevated temperatures in the RN-17B TEE extrusive lithologies is also unique. Overprinting of in situ oceanic crust that experienced axial hydrothermal alteration by subsequent low-temperature alteration has been widely discussed. The RN-17B rocks raise the possibility that underprinting of high-temperature alteration by earlier low-temperature alteration may also be a factor in mass exchange estimates at locations where oceanic crust is volcanically thickened and has subsided.

4.4.3. Rare Earth Elements

LREE are generally enriched in oceanic crust that has undergone low-temperature weathering by seawater [*Thompson*, 1973; *Ludden and Thompson*, 1979; *Staudigel et al.*, 1995, 1996]. LREE gains have also been documented for chloritized pillow basalt margins that have undergone higher temperature (200–380°C) hydrothermal alteration in Hole 856 at Middle Valley [*Teagle and Alt*, 2004], along with samples from the upper sheeted dikes in Hole 504B [*Alt and Emmerman*, 1985; *Alt et al.*, 1985]. REE are generally immobile during the low-temperature palagonitization of basaltic glass by seawater [*Pauly et al.*, 2011], so while LREE gains appear to occur at a range of temperatures and conditions, REE loss from rocks unlikely stems from low-temperature oxidative weathering processes. The source of the LREE remains an active area of research. Few examples of LREE-depleted rocks from the oceanic crust have previously been recovered. Exceptions that show preferential mobilization of LREE relative to HREE include extensively altered patches at the base of the Hole 504B drill core that show up to 50% lower REE than surrounding weakly altered dolerite [*Bach and Irber*, 1998], and a chloritized pillow margin and wall rock sample from the pillow basalt—sheeted dike transition in Hole 504B [*Alt and Emmerman*, 1985].

The LREE depletion of hornblende replacing glassy pillow rinds and hyaloclastite shards in RN-17B relative to whole-rock samples (Figure 7) is similar to the few examples of LREE-depleted rocks from in situ oceanic crust. LREE loss likely reflects a combination of increased stability of LREE (particularly La^{3+} and Eu^{2+}) aqueous chloride complexes in chloride-rich fluids at temperatures above 250°C that more readily leach LREE from reactive portions of rocks [*Allen and Seyfried*, 2005; *Migdisov et al.*, 2009]. The LREE gains and losses in RN-17B rocks are related to domains of variable initial porosity, providing an example of high fluid flow at elevated temperatures providing an important control on REE leaching.

4.4.4. Cu, Zn, and Pb

Cu and Zn loss observed in lower sheeted dikes from in situ oceanic crust is attributed to leaching in the high temperature ($>350°C$) hydrothermal root zone. A later stage of alteration resulted in Cu and Zn sulfide precipitation and enrichment in the upper sheeted dikes (e.g., ODP/IODP Hole 504B [*Alt et al.*, 1996], ODP/

IODP Hole 1256D [*Alt et al.*, 2010], Hess Deep [*Gillis*, 1995], and Pito Deep [*Heft et al.*, 2008]). The lack of Cu depletion in RN-30 dolerites, coupled with chalcopyrite occurrence on fracture surfaces, suggests Cu was mobilized from a deeper source and precipitated at the in situ temperature of 345°C. This is consistent with the observation of *Libbey and Williams-Jones* [2016] that secondary chalcopyrite (with pyrite or pyrrhotite) is widely distributed in the Reykjanes geothermal reservoir rocks.

Pb isotope studies of seafloor basalts, massive sulfide deposits, and metalliferous sediments demonstrate that Pb is readily leached from MORB at depth in the oceanic crust [*Brévart et al.*, 1981; *Vidal and Clauer*, 1981; *Peucker-Ehrenbrink et al.*, 1994; *Chauvel et al.*, 1995; *Fouquet and Marcoux*, 1995; *Fouquet et al.*, 1996]. Zn and Pb concentrations are highly covariable in axial and off-axis hydrothermal massive sulfide deposits [*Zierenberg et al.*, 1984; *Doe*, 1994; *Fouquet et al.*, 1996], while Cu does not typically covary with Zn and Pb [*Doe*, 1994]. In seafloor hydrothermal fluids, Cu is decoupled from Zn and Pb owing to much lower solubility of Cu sulfide relative to Zn and Pb sulfide for a given temperature [*Zierenberg et al.*, 1984]. Cu solubility is controlled by chalcopyrite supersaturation at <350°C [*Seewald and Seyfried*, 1990; *Seyfried and Ding*, 1995] and Zn solubility is controlled by sphalerite supersaturation at <250°C [*Janecky and Seyfried*, 1984]. Cu is enriched in RN-30 dolerites based on the widespread occurrence of chalcopyrite in veins not included in whole-rock analyses, but in contrast to RN-17B, Zn and Pb are not enriched because temperatures experienced by the dikes in RN-30 remain too hot to precipitate Zn and Pb sulfides.

The gains of U, Mg, Pb, and Zn (and possibly LREE) in extrusive RN-17B and RN-30 rocks are consistent with low-temperature weathering/alteration upper portions of the oceanic crust. In contrast, higher-temperature mineral assemblages (greenschist and amphibole grade) and losses of alkalis, Ba, and Cu (and LREE in two samples) recorded by the RN-17B extrusive rocks are characteristic of higher-temperature samples recovered from the sheeted dike section on the ocean floor, particularly at the base of Hole 504B as described by *Alt et al.* [1986].

5. Summary

Figure 11 is a schematic diagram depicting element gains and losses recorded by TEE rocks in the RN-17B and RN-30 cores. Rocks in the RN-17B core were originally emplaced on the seafloor, subsided due to down-faulting and lithospheric subsidence, and were buried by continued volcanism [*Björnsson et al.*, 1972; *Friðleifsson and Richter*, 2010; *Fowler et al.*, 2015]. The RN-17B rocks record a complex history of elemental gains and losses that involved several stages of alteration. The first stage occurred at low temperature after initial emplacement on the seafloor, and is recorded by addition of seawater uranium to the rocks. Alteration at increasingly elevated temperatures is reflected by gain of Mg (and likely gains of alkalis and Ba in clay minerals) in smectite clays. The second stage of alteration occurred at >200°C, when alkalis and Ba were remobilized during the breakdown of smectite clays to form chlorite. LREE were potentially lost at this stage from rocks that experienced high effective water-rock ratios, or were potentially lost during a subsequent stage of higher-temperature alteration. Seawater Mg continued to be added to the rocks and was hosted by chlorite. More advanced alteration (Stage 3) involved temperatures that likely exceeded 400°C and is recorded by loss of Cu (likely coupled with Zn and Pb depletion). This higher temperature >400°C alteration stage is also evident based on fluid inclusions in epidote veins in the RN-17B core, which correspond to a boiling event likely induced by intrusion of a dike [*Fowler et al.*, 2015]. Cuttings from RN-17 also record localized high temperature (>950°C) pyroxene hornfels alteration [*Marks et al.*, 2011]. Zn and Pb enrichment in RN-17B suggest an episode of lower temperature fluid flow capable of depositing Pb and Zn sulfide.

Alteration even more extreme than that recorded by the RN-17B hyaloclastite samples was documented in hyaloclastite samples recovered from RN-30, where altered basalt shows extensive silicification (>70 wt % SiO_2). In contrast, elemental gains and losses recorded by dolerite in the RN-30 core are more modest and can be explained by a single stage of alteration at or above the in situ temperature of 345°C, temperatures too hot to deposit Pb or Zn sulfide. Loss of Rb, K, Ba, and Pb from RN-30 dolerite is accompanied by slight Cu gain in mineralized fractures. The lack of Mg and U enrichment in RN-30 dolerite suggests that the hydrothermal fluid is evolved seawater depleted in these elements earlier in the flow path. Elemental gains and losses in the RN-30 core and the low degree of alteration of primary plagioclase and clinopyroxene in
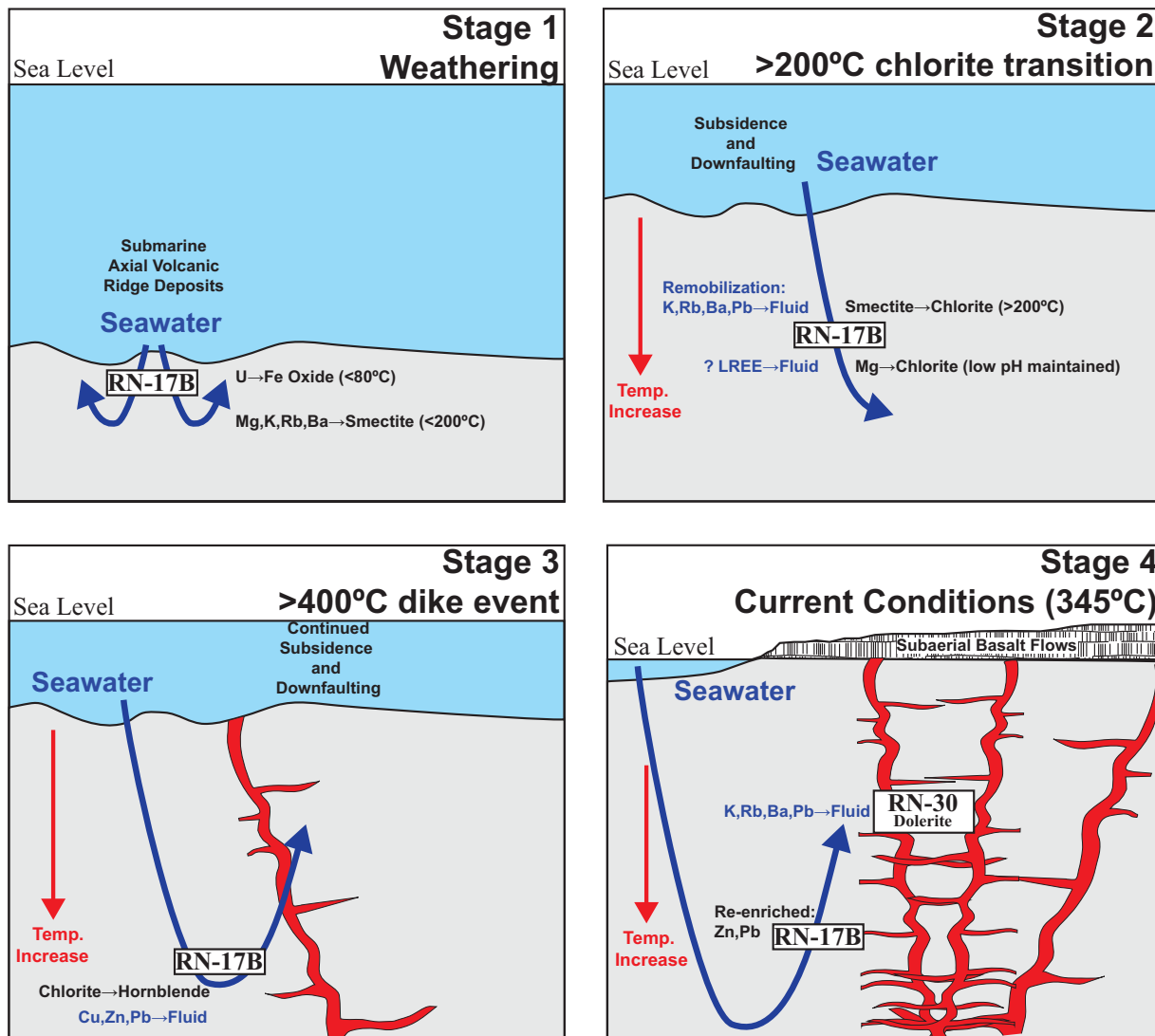
Figure 11. Schematic diagram depicting stages of alteration recorded by extrusive rocks in the RN-17B core and intrusive rocks in the RN-30 core. Text in blue indicates elements lost from rock to fluid, text in black indicates elements gained by rock from fluids.

the core is consistent with emplacement as intrusions relatively recently near the current depth. It is only by analysis of drill core that the multistage history of alteration in this active geothermal system can be ascertained.

6. Conclusions

Elemental gains and losses resulting from hydrothermal fluid-rock reactions is a processes of global significance. Chemical reactions occurring in the active roots of hydrothermal systems set the composition of hydrothermal vent fluids, and thus provide an important control on seawater chemistry. These reactions also modify the composition of oceanic crust, which is ultimately recycled in subduction zones. The Reykjanes drill cores are unique in that they were recovered at high temperature from an active, basalt-hosted, seawater-recharged geothermal system. Elemental gains and losses recorded by the RN-30 intrusive basalts are consistent with observations from the upper sheeted dike section drilled from in situ oceanic crust in several locations. The RN-17B lithologies and the RN-30 hyaloclastites that were originally emplaced on the seafloor record the integrated effects of elemental gains and losses imprinted during subsidence through increasingly elevated temperatures. Elemental gains and losses in the altered rocks are comparable to hydrothermal element gains and losses that occur at various stages of hydrothermal alteration beneath

submarine hydrothermal systems. While late-stage retrograde hydrothermal alteration has not "overprinted" the rocks in the RN-17B drill cores, early stage alteration "underprints" high-temperature alteration in many of the extrusive samples.

References

Allen, D. E., and W. E. Seyfried (2005), REE controls in ultramafic hosted MOR hydrothermal systems: An experimental study at elevated temperature and pressure, *Geochim. Cosmochim. Acta*, *69*(3), 675–683.

Alt, J. C. et al. (1996), Hydrothermal alteration of a section of upper oceanic crust in the eastern equatorial Pacific: a synthesis of results from Site 504 (DSDP Legs 69, 70, and 83, and ODP Legs 111, 137, 140, and 148.), in *Proceedings of the Ocean Drilling Program*, edited by J. C. Alt et al., pp. 417–434, Scientific Results, College Station, Tex.

Alt, J. C. (1995), Subseafloor processes in mid-ocean ridge hydrothermal systems, in *Seafloor Hydrothermal Systems: Physical, Chemical, Biological, and Geological Interactions, Geophys. Monogr. Ser*., edited by S. E. Humphris et al., pp. 85–113, AGU, Washington, D. C.

Alt, J. C., and R. Emmerman (1985), Geochemistry of hydrothermally altered basalts—Deep Sea Drilling Project Hole 504B, Leg 83, in *Initial Reports of the Deep Sea Drilling Project*, vol. 83, edited by J. Anderson, J. Honnorez, and K. Becker, pp. 249–262, U.S. Gov. Print. Off., Washington, D. C.

Alt, J. C., and D. A. H. Teagle (1999), The uptake of carbon during alteration of the ocean crust, *Geochim. Cosmochim. Acta*, *63*(10), 1527–1535.

Alt, J. C., C. Laverne, and K. Muehlenbachs (1985), Alteration of the upper oceanic crust: Mineralogy and processes in Deep Sea Drilling Project Hole 504B, Leg 83, in *Initial Reports of the Deep Sea Drilling Project*, vol. 83, edited by J. Anderson, J. Honnorez, and K. Becker, pp. 217–247, U.S. Gov. Print. Off., Washington, D. C.

Alt, J. C., J. Honnorez, C. Laverne, and R. Emmerman (1986), Hydrothermal alteration of a 1 km section through the upper oceanic crust, deep sea drilling project Hole 504B: Mineralogy, chemistry, and evolution of seawater basalt intrusions, *J. Geophys. Res.*, *91*(B10), 10,309–10,335.

Alt, J. C., C. Laverne, R. M. Coggon, D. A. H. Teagle, N. R. Banerjee, S. Morgan, C. E. Smith-Duque, M. Harris, and L. Galli (2010), Subsurface structure of a submarine hydrothermal system in ocean crust formed at the East Pacific Rise, ODP/IODP Site 1256, *Geochem. Geophys. Geosyst.*, *11*, Q10010, doi:10.1029/2010GC003144.

Ármannsson, H. (2016), The fluid geochemistry of Icelandic high temperature geothermal areas, *Appl. Geochem.*, *66*, 14–64.

Arnórsson, S. (1978), Major element chemistry of the geothermal sea-water at Reykjanes and Svartsengi, Iceland, *Mineral. Mag.*, *42*, 209–220.

Arnórsson, S. (1995), Geothermal systems in Iceland: Structure and conceptual models I. High temperature areas, *Geothermics*, *24*(5/6), 561–602.

Bach, W., and W. Irber (1998), Rare earth element mobility in the oceanic lower sheeted dike complex: Evidence from geochemical data and leaching experiments, *Chem. Geol.*, *151*, 309–326.

Bach, W., J. C. Alt, Y. Niu, S. E. Humphris, J. Erzinger, and H. J. B. Dick (2001), The geochemical consequences of late-stage low-grade alteration of lower ocean crust at the SW Indian Ridge: Results from ODP hole 735B (Leg 176), *Geochim. Cosmochim. Acta*, *65*(19), 3267–3287.

Bach, W., B. Peucker-Ehrenbrink, S. R. Hart, and J. S. Blusztajn (2003), Geochemistry of hydrothermally altered oceanic crust: DSDP/ODP Hole 504B—Implications for seawater-crust exchange budgets and Sr- and Pb-isotopic evolution of the mantle, *Geochem. Geophys. Geosyst.*, *4*(3), 8904, doi:10.1029/2002GC000419.

Barrett, T. J., and W. H. MacLean (1994), Chemostratigraphy and hydrothermal alteration in exploration of for VHMS deposits in greenstones and younger volcanic rocks, in *Alteration and Alteration Processes Associated With Ore Forming Systems, Short Course Notes*, edited by D. R. Lenz, vol. 11, pp. 433–467, Geol. Assoc. of Can., Waterloo, Ontario.

Becker, K., et al. (1989), Drilling deep into young oceanic crust, Hole 504B, Costa Rica Rift, *Rev. Geophys.*, *27*, 79–102.

Bischoff, J. L., and F. W. Dickson (1975), Seawater-basalt interaction at 200°C and 500 bars: Implications for origin of sea-floor heavy metal deposits and regulation of seawater chemistry, *Earth Planet. Sci. Lett.*, *25*, 385–397.

Bjornsson, S., S. Arnorsson, and J. Tomasson (1972), Economic evaluation of Reykjanes thermal brine area, Iceland, *Am. Assoc. Pet. Geol. Bull.*, *56*, 2380–2391.

Bloch, S., and A. W. Hofmann (1978), Magnesium metasomatism during hydrothermal alteration of new oceanic crust, *Geology*, *6*, 275–277.

Brandon, A. D., D. W. Graham, T. Waight, and B. Gautason (2007), [186]Os and [187]Os enrichments and high-3He/4He sources in the Earth's mantle: Evidence from Icelandic picrites, *Geochim. Cosmochim. Acta*, *71*(18), 4570–4591.

Brévart, O., B. Dupré, and C. J. Allegré (1981), Metallogenesis at spreading centers: Lead isotope systematics for sulfides, manganses-rich crusts, basalts, and sediments from the Cyamix and Alvin areas (East Pacific Rise), *Econ. Geol.*, *76*(5), 1205–1210.

Chauvel, C., and C. Hémond (2000), Melting of a complete section of recycled oceanic crust: Trace element and Pb isotopic evidence from Iceland, *Geochem. Geophys. Geosyst.*, *1*(2), 1001.

Chauvel, C., S. L. Goldstein, and A. W. Hofmann (1995), Hydration and dehydration of oceanic crust controls on Pb evolution of the crust, *Chem. Geol.*, *126*, 65–75.

Chen, J. H., G. J. Wasserburg, K. L. Von Damm, and J. M. Edmond (1986), The U-Th-Pb systematics in hot springs on the East Pacific Rise at 21 N and Guaymas Basin, *Geochim. Cosmochim. Acta*, *50*, 2467–2479.

Clifton, A. E., and S. A. Kattenhorn (2006), Structural architecture of a highly oblique divergent plate boundary segment, *Tectonophysics*, *419*(1–4), 27–40.

Dekkers, M. J., D. Heslop, E. Herrero-Bervera, G. Acton, and D. Krasa (2014), Insights into magmatic processes and hydrothermal alteration of in situ superfast spreading ocean crust at ODP:IODP site 1256 from a cluster analysis of rock magnetic properties, *Geochem. Geophys. Geosyst.*, *15*, 3430–3447, doi:10.1002/2014GC005343.

Doe, B. R. (1994), Zinc, copper, and lead in mid-ocean ridge basalts and the source rock control on Zn/Pb in ocean-ridge hydrothermal deposits, *Geochim. Cosmochim. Acta*, *58*(10), 2215–2223.

Edmond, J. M., C. I. Measures, R. E. McDuff, L. H. Chan, R. Collier, B. Grant, L. I. Gordon, and J. B. Corliss (1979), Ridge crest hydrothermal activity and the balances of the major and minor elements in the ocean: The Galapagos data, *Earth Planet. Sci. Lett.*, *46*, 1–18.

Einarsson, P., and K. Sæmundsson (1987), Earthquake epicenters 1982–1985 and volcanic systems in Iceland (map), in *Í Hlutarsins Eðli: Festschrift for Thorbjorn Sigurgeirsson*, edited by Th. Sigfússon, Menningarsjóður, Reykjavík.

Elderfield, H., E. Gunnlaugsson, S. J. Wakefield, and P. T. Williams (1977), The geochemistry of basalt-seawater interactions: Evidence from Deception Island, Antarctica and Reykjanes, Iceland, *Mineral. Mag.*, *41*, 217–226.

Elliott, T. R., C. J. Hawkesworth, and K. Grönvold (1991), Dynamic melting of the Iceland plume, *Nature*, *351*, 201–206.

Fitton, J. G. (2003), Does depleted mantle form an intrinsic part of the Iceland plume?, *Geochem. Geophys. Geosyst.*, *4*(3), 1032, doi:10.1029/2002GC000424.

Floyd, P. A., and J. A. Winchester (1978), Identification and discrimination of altered and metamorphosed volcanic rocks using immobile elements, *Chem. Geol.*, *21*, 291–306.

Fouquet, Y., and E. Marcoux (1995), Lead isotope systematics in Pacific hydrothermal sulfide deposits, *J. Geophys. Res.*, *100*(B4), 6025–6040.

Fouquet, Y., R. Knott, P. Cambon, A. E. Fallick, D. Rickard, and D. Desbruyeres (1996), Formation of large sulfide mineral deposits along fast spreading ridges. Example from off-axial deposits at 12.43′N on the East Pacific Rise, *Earth Planet. Sci. Lett.*, *144*, 147–162.

Fowler, A. P. G., and R. A. Zierenberg (2016), Geochemical bias in drill cutting samples versus drill core samples returned from the Reykjanes Geothermal System, Iceland, *Geothermics*, *62*, 48–60.

Fowler, A. P. G., R. A. Zierenberg, P. Schiffman, N. Marks, and G. Ó. Friðleifsson (2015), Evolution of fluid–rock interaction in the Reykjanes geothermal system, Iceland: Evidence from Iceland Deep Drilling Project core RN-17B, *J. Volcanol. Geotherm. Res.*, *302*, 47–63.

Franzson, H., S. Thordarson, G. Bjornsson, S. Gudlaugsson, B. Richter, G. Friðleifsson, and S. Thorhalsson (2002), Reykjanes high-temperature field, SW-Iceland. Geology and hydrothermal alteration of well RN-10, in *27th Stanford Workshop on Geothermal Reservoir Engineering*, pp. 233–240, Stanford University, Stanford, Calif.

Franzson, H., R. Zierenberg, and P. Schiffman (2008), Chemical transport in geothermal systems in Iceland. *Evidence from hydrothermal alteration, J. Volcanol. Geotherm. Res.*, *173*(3–4), 217–229.

Freedman, A. J. E., D. K. Bird, S. Arnorsson, T. Fridriksson, W. A. Elders, and G. O. Friðleifsson (2009), Hydrothermal minerals record CO$_2$ partial pressures in the Reykjanes geothermal system, Iceland, *Am. J. Sci.*, *309*, 788–833.

Friðleifsson, G. Ó., and B. Richter (2010), The geological significance of two IDDP-ICDP spot cores from the Reykjanes geothermal field, Iceland, in *Proceedings of World Geothermal Congress*, pp. 1–7, International Geothermal Association, Bochum, Germany.

Friðleifsson, G. O., et al. (2005), Reykjanes well report RN-17 and RN-17ST, *Tech. Rep. ISOR-2005/007*, Iceland Geosurv., Reykjavik.

Friðleifsson, G. Ó., A. Albertsson, W. Elders, Ó. Sigurdsson, R. Karlsdottir, and B. Pálsson (2011), The Iceland Deep Drilling Project (IDDP): Planning for the second deep well at Reykjanes, *Geotherm. Resour. Counc. Trans.*, *35*, 347–354.

Friðleifsson, G. Ó., W. A. Elders, and A. Albertsson (2014), The concept of the Iceland deep drilling project, *Geothermics*, *49*, 2–8.

Gee, M. A. M., M. F. Thirlwall, R. N. Taylor, D. Lowry, and B. J. Murton (1998), Crustal processes: Major controls on Reykjanes Peninsula lava chemistry, SW Iceland, *J. Petrol.*, *39*(5), 819–839.

Gillis, K. M. (1995), Controls on hydrothermal alteration in a section of fast-spreading oceanic crust, *Earth Planet. Sci. Lett.*, *134*(3–4), 473–489.

Gillis, K. M. (1996), Rare earth element constraints on the origin of amphibole in gabbroic rocks from site 894, Hess Deep, in *Proceedings of the Ocean Drilling Program, Scientific Results*, vol. 147, pp. 59–75, Ocean Drill. Program, College Station, Tex.

Grant, J. A. (1986), The isocon diagram—A simple solution to Gresens' equation for metasomatic alteration, *Econ. Geol.*, *81*, 1976–1982.

Gresens, R. L. (1967), Composition-volume relationships of metasomatism, *Chem. Geol.*, *2*, 47–65.

Gudmundsson, A., F. A. Pasquarè Mariotto, and A. Tibaldi (2014), Dykes, sills, laccoliths and inclined sheets in Iceland, in *Advances in Volcanology, Laccoliths, Sills and Dykes, Physical Geology of Shallow Level Magmatic Systems*, pp. 1–14, Springer, Berlin.

Günther, D., and B. Hattendorf (2005), Solid sample analysis using laser ablation inductively coupled plasma mass spectrometry, *Trends Anal. Chem.*, *24*, 255–265.

Gurenko, A. A., and M. Chaussidon (1995), Enriched and depleted primitive melts included in olivine from Icelandic tholeiites: Origin by continuous melting of a single mantle column, *Geochim. Cosmochim. Acta*, *59*(14), 2905–2917.

Hajash, A. (1975), Hydrothermal processes along mid-ocean ridges: An experimental investigation, *Contrib. Mineral. Petrol.*, *53*, 205–226.

Hanan, B. B., and J. G. Schilling (1997), The dynamic evolution of the Iceland mantle plume: The lead isotope perspective, *Earth Planet. Sci. Lett.*, *151*, 43–60.

Hardardóttir, H., K. L. Brown, Th. Fridriksson, J. W. Hedenquist, M. D. Hannington, and S. Thorhallsson (2009), Metals in deep liquids of the Reykjanes geothermal system, southwest Iceland: Implications for the compositions of seafloor black smoker fluids, *Geology*, *37*, 1103–1106.

Hardardóttir, H., M. Hannington, J. Hedenquist, I. Kjarsgaard, and K. Hoal (2012), Cu-rich scales in the Reykjanes geothermal system, *Econ. Geol.*, *105*, 1143–1155.

Hart, R. (1970), Chemical exchange between sea water and deep ocean basalts, *Earth Planet. Sci. Lett.*, *9*, 269–279.

Hart, S. R. (1969), K, Rb, Cs contents and K/Rb, K/Cs ratios of fresh and altered submarine basalts, *Earth Planet. Sci. Lett.*, *6*, 295–303.

Hart, S. R., and H. Staudigel (1982), The control of alkalis and uranium in seawater by ocean crust alteration, *Earth Planet. Sci. Lett.*, *58*, 202–212.

Hart, S. R., J. G. Schilling, and J. L. Powell (1973), Basalts from Iceland and along the Reykjanes Ridge: Sr isotope geochemistry, *Nat. Phys. Sci.*, *246*, 104–107.

Hart, S. R., J. Blusztajn, H. J. B. Dick, P. S. Meyer, and K. Muehlenbachs (1999), The fingerprint of seawater circulation in a 500-meter section of ocean crust gabbros, *Geochim. Cosmochim. Acta*, *63*, 4059–4080.

Heft, K. L., K. M. Gillis, M. A. Pollock, J. A. Karson, and E. M. Klein (2008), Role of upwelling hydrothermal fluids in the development of alteration patterns at fast spreading ridges: Evidence from the sheeted dike complex at Pito Deep, *Geochem. Geophys. Geosyst.*, *9*, Q05O07, doi:10.1029/2007GC001926.

Hemond, C., N. T. Arndt, U. Lichtenstein, A. W. Hofmann, N. Oskarsson, and S. Steinthorsson (1993), The heterogeneous Iceland plume: Nd-Sr-O isotopes and trace element constraints, *J. Geophys. Res.*, *98*(B9), 15,833–15,850.

Huang, J., S. Ke, Y. Gao, Y. Xiao, and S. Li (2015), Magnesium isotopic compositions of altered oceanic basalts and gabbros from IODP site 1256 at the East Pacific Rise, *Lithos*, *231*, 53–61.

Humphris, S. E., and G. Thompson (1978a), Hydrothermal alteration of oceanic basalts by seawater, *Geochim. Cosmochim. Acta*, *42*, 107–125.

Humphris, S. E., and G. Thompson (1978b), Trace element mobility during hydrothermal alteration of oceanic basalts, *Geochim. Cosmochim. Acta*, *42*, 127–136.

Humphris, S. E., A. Morrison, and R. N. Thompson (1978), Influence of rock crystallisation history upon subsequent lanthanide mobility during hydrothermal alteration of basalts, *Chem. Geol.*, *23*, 125–137.

Ildefonse, B., P. A. Rona, and D. Blackman (2007), Drilling the crust at mid-ocean ridges, *Oceanography*, *20*(1), 66–77.

Jakobsson, S. P., J. Jonsson, and F. Shido (1978), Petrology of the western Reykjanes Peninsula, Iceland, *J. Petrol.*, *19*(4), 669–705.

Janecky, D. R., and W. E. Seyfried Jr. (1984), Formation of massive sulfide deposits on oceanic ridge crests: Incremental reaction models for mixing between hydrothermal solutions and water, *Geochim. Cosmochim. Acta*, *48*, 2723–2738.

Jenner, G. A., H. P. Longerich, S. E. Jackson, and B. J. Fryer (1990), ICP-MS-A powerful tool for high-precision trace-element analysis in Earth sciences: Evidence from analysis of selected U.S.G.S. reference samples, *Chem. Geol.*, *83*, 133–148.

Jochum, K. P., H. M. Seufert, and M. F. Thirlwall (1990), High-sensitivity Nb analysis by spark-source mass spectrometry (SSMS) and calibration of XRF Nb and Zr, *Chem. Geol.*, *81*, 1–16.

Jochum, K. P., et al. (2006), MPI-DING reference glasses for in situ microanalysis: New reference values for element concentrations and isotope ratios, *Geochem. Geophys. Geosyst.*, *7*, Q02008, doi:10.1029/2005GC001060.

Johnson, D. M., P. R. Hooper, and R. M. Conrey (1999), XRF analysis of rocks and minerals for major and trace elements on a single low dilution Li-tetraborate fused bead, *Adv. X-ray Anal.*, *41*, 843–867.

Joron, J. L., L. Briqueu, H. Bougault, and M. Treuil (1980), East Pacific Rise, Galapagos spreading center and Siqueiros Fracture Zone, Deep Sea Drilling Project, Project Leg 54: Hygromagmaphile elements—A comparison with the North Atlantic, in *Initial Reports of the Deep Sea Drilling Project*, vol. 54, pp. 725–735, U.S. Gov. Print. Off., Washington, D. C.

Kempton, P. D., J. G. Fitton, A. D. Saunders, G. M. Nowell, R. N. Taylor, B. S. Hardarson, and G. Pearson (2000), The Iceland plume in space and time—A Sr-Nd-Pb-Hf study of the North Atlantic rifted margin, *Earth Planet. Sci. Lett.*, *177*, 255–271.

Kokfelt, T. F. (2006), Combined trace element and Pb-Nd-Sr-O isotope evidence for recycled oceanic crust (upper and lower) in the Iceland mantle plume, *J. Petrol.*, *47*(9), 1705–1749.

Koornneef, J. M., A. Stracke, B. Bourdon, M. A. Meier, K. P. Jochum, B. Stoll, and K. Gronvold (2012), Melting of a two-component source beneath Iceland, *J. Petrol.*, *53*(1), 127–157.

Kurnosov, V. B., B. P. Zolotarev, A. V. Artamonov, S. M. Lyapunov, G. L. Kashintsev, O. V. Chudaev, A. L. Sokolova, and S. A. Garanina (2008), *Geochemistry of the Oceanic Crust From Ocean Drilling Samples*, 1046 p., Russ. Acad. of Sci., Moscow.

Laverne, C., P. Agrinier, D. Hermitte, and M. Bohn (2001), Chemical fluxes during hydrothermal alteration of a 1200-m long section of dikes in the oceanic crust, DSDP/ODP hole 504B, *Chem. Geol.*, *181*, 73–98.

Libbey, R. B., and A. E. Williams-Jones (2016), Relating sulfide mineral zonation and trace element chemistry to subsurface processes in the Reykjanes geothermal system, Iceland, *J. Volcanol. Geotherm. Res.*, *310*, 225–241.

Longerich, H. P., S. E. Jackson, and D. Gunther (1996), Laser ablation inductively coupled plasma mass spectrometric transient signal data acquisition and analyte concentration calculation, *J. Anal. At. Spectrom.*, *11*, 899–904.

Lonker, S. W., H. Franzson, and H. Kristmannsdottir (1993), Mineral fluid interactions in the Reykjanes and Svartsengi geothermal systems, *Am. J. Sci.*, *293*, 605–670.

Ludden, J. N., and G. Thompson (1979), An evaluation of the behavior of the rare earth elements during the weathering of sea-floor basalt, *Earth Planet. Sci. Lett.*, *43*, 85–92.

Marks, N., P. Schiffman, R. Zierenberg, H. Franzson, and G. Ó. Friðleifsson (2010), Hydrothermal alteration in the Reykjanes geothermal system: Insights from Iceland deep drilling program well RN-17, *J. Volcanol. Geotherm. Res.*, *189*(1–2), 172–190.

Marks, N., P. Schiffman, and R. A. Zierenberg (2011), High-grade contact metamorphism in the Reykjanes geothermal system: Implications for fluid-rock interactions at mid-oceanic ridge spreading centers, *Geochem. Geophys. Geosyst.*, *12*, Q08007, doi:10.1029/2011GC003569.

Marks, N., R. A. Zierenberg, and P. Schiffman (2015), Strontium and oxygen isotopic profiles through 3 km of hydrothermally altered oceanic crust in the Reykjanes Geothermal System, Iceland, *Chem. Geol.*, *412*, 34–47.

Martin, E., and O. Sigmarsson (2010), Thirteen million years of silicic magma production in Iceland: Links between petrogenesis and tectonic settings, *Lithos*, *116*, 129–144.

McDonough, W. F., and S. S. Sun (1995), The composition of the Earth, *Chem. Geol.*, *120*, 223–253.

Michard, A. (1989), Rare earth element systematics in hydrothermal fluids, *Geochim. Cosmochim. Acta*, *53*, 745–750.

Migdisov, A. A., A. E. Williams-Jones, and T. Wagner (2009), An experimental study of the solubility and speciation of the Rare Earth Elements (III) in fluoride- and chloride-bearing aqueous solutions at temperatures up to 300°C, *Geochim. Cosmochim. Acta*, *73*(23), 7087–7109.

Mortensen, A. K., et al. (2006), Well report for RN-19 [in Icelandic], *Icelandic Geosurv. Rep. ISOR-2006/025*, 139 pp.

Mottl, M. J. (1983), Metabasalts, axial hot springs, and the structure of hydrothermal systems at mid-ocean ridges, *Geol. Soc. Am. Bull.*, *94*(2), 161–180.

Mottl, M. J., and H. D. Holland (1978), Chemical exchange during hydrothermal alteration of basalt by seawater-I. Experimental results for major and minor components of seawater, *Geochim. Cosmochim. Acta*, *42*, 1103–1115.

Mottl, M. J., and C. G. Wheat (1994), Hydrothermal circulation through mid-ocean ridge flanks: Fluxes of heat and magnesium, *Geochim. Cosmochim. Acta*, *58*, 2225–2237.

Murton, B. J., R. N. Taylor, and M. F. Thirlwall (2002), Plume-ridge interaction: A geochemical perspective from the Reykjanes Ridge, *J. Petrol.*, *43*(11), 1987–2012.

Nielsen, S. G., M. Rehkämper, A. D. Brandon, M. D. Norman, S. Turner, and S. Y. O'Reilly (2007), Thallium isotopes in Iceland and Azores lavas—Implications for the role of altered crust and mantle geochemistry, *Earth Planet. Sci. Lett.*, *264*(1–2), 332–345.

Nozaka, T., and P. Fryer (2011), Alteration of the oceanic lower crust at a slow-spreading axis: Insight from vein-related zoned halos in olivine gabbro from Atlantis Massif, Mid-Atlantic Ridge, *J. Petrol.*, *52*, 643–664.

Ólafsson, J., and J. P. Riley (1978), Geochemical studies on the thermal brine from Reykjanes, Iceland, *Chem. Geol.*, *21*, 219–237.

Oskarsson, N., S. Steinthorsson, and G. E. Sigvaldason (1985), Iceland geochemical anomaly: Origin, volcanotectonics, chemical fractionation and isotope evolution of the crust, *J. Geophys. Res.*, *90*(B12), 10,011–10,025.

Parson, L. M., et al. (1993), En echelon axial volcanic ridges at the Reykjanes Ridge: A life cycle of volcanism and tectonics, *Earth Planet. Sci. Lett.*, *117*, 73–87.

Paton, C., J. Hellstrom, B. Paul, J. Woodhead, and J. Hergt (2011), Iolite: Freeware for the visualisation and processing of mass spectrometric data, *J. Anal. At. Spectrom.*, *26*(12), 2508–2518.

Pauly, B. D., P. Schiffman, R. A. Zierenberg, and D. A. Clague (2011), Environmental and chemical controls on palagonitization, *Geochem. Geophys. Geosyst.*, *12*, Q12017, doi:10.1029/2011GC003639.

Peate, D. W., J. A. Baker, S. P. Jakobsson, T. E. Waight, A. J. R. Kent, N. V. Grassineau, and A. C. Skovgaard (2009), Historic magmatism on the Reykjanes Peninsula, Iceland: A snap-shot of melt generation at a ridge segment, *Contrib. Mineral. Petrol.*, *157*(3), 359–382.

Peate, D. W., K. Breddam, J. A. Baker, M. D. Kurz, A. K. Barker, T. Prestvik, N. Grassineau, and A. C. Skovgaard (2010), Compositional characteristics and spatial distribution of enriched Icelandic mantle components, *J. Petrol.*, *51*(7), 1447–1475.

Peucker-Ehrenbrink, B., A. W. Hofmann, and R. Hart (1994), Hydrothermal lead transfer from mantle to continental crust: The role of metalliferous sediments, *Earth Planet. Sci. Lett.*, *125*, 129–142.

Pope, E. C., D. K. Bird, S. Arnórsson, T. Fridriksson, W. A. Elders, and G. Ó. Friðleifsson (2009), Isotopic constraints on ice age fluids in active geothermal systems: Reykjanes, Iceland, *Geochim. Cosmochim. Acta*, *73*(15), 4468–4488.

Reed, M. (1983), Seawater-basalt reaction and the origin of greenstones and related ore deposits, *Econ. Geol.*, *78*, 466–485.

Revillon, S., N. T. Arndt, E. Hallot, A. C. Kerr, and J. Tarney (1999), Petrogenesis of picrites from the Caribbean Plateau and the North Atlantic magmatic province, *Lithos*, *49*, 1–21.

Sæmundsson, K. (1979), Outline of the geology of Iceland, *Jökull*, *29*, 7–28.

Schilling, J. G. (1973), Iceland mantle plume: A geochemical study of the Reykjanes Ridge, *Nature*, *242*, 565–571.

Seewald, J. S., and W. E. Seyfried Jr. (1990), The effect of temperature on metal mobility in subseafloor hydrothermal systems: Constraints from basalt alteration experiments, *Earth Planet. Sci. Lett.*, *101*, 308–403.

Seyfried, W. E., Jr. (1987), Experimental and theoretical constraints on hydrothermal alteration processes at mid-ocean ridges, *Annu. Rev. Earth Planet. Sci.*, *15*, 317–335.

Seyfried, W. E., Jr., and J. L. Bischoff (1979), Low temperature basalt interaction with seawater: An experimental study at 70°C and 150°C, *Geochim. Cosmochim. Acta*, *43*, 1937–1947.

Seyfried, W. E., Jr., and J. L. Bischoff (1981), Experimental seawater-basalt interaction at 300°C, 500 bars, chemical exchange, secondary mineral formation and implications for the transport of heavy metals, *Geochim. Cosmochim. Acta*, *45*(2), 135–147.

Seyfried, W. E., and K. Ding (1995), Phase equilibria in subseafloor hydrothermal systems: A review of the role of redox, temperature, pH and dissolved Cl on the chemistry of hot spring fluids at mid-ocean ridges, in *Seafloor Hydrothermal Systems: Physical, Chemical, Biological, and Geological Interactions, Geophys. Monogr. Ser.*, edited by S. E. Humphris et al., vol. 91, pp. 248–272, AGU, Washington, D. C.

Seyfried, W. E., Jr., and M. J. Mottl (1982), Hydrothermal alteration of basalt by seawater under seawater-dominated conditions, *Geochim. Cosmochim. Acta*, *46*, 985–1002.

Skinner, A. C., P. Bowers, S. Þórhallsson, G. Ó. Friðleifsson, and H. Guðmundsson (2010), Design, manufacture, and operation of a core barrel for the Iceland Deep Drilling Project (IDDP), *Sci. Drill.*, *10*, 40–45.

Skovgaard, A. C., M. Storey, J. Baker, J. Blusztajn, and S. R. Hart (2001), Osmium-oxygen isotopic evidence for a recycled and strongly depleted component in the Iceland mantle plume, *Earth Planet. Sci. Lett.*, *194*, 259–275.

Staudigel, H., and S. R. Hart (1983), Alteration of basaltic glass: Mechanisms and significance for the oceanic crust-seawater budget, *Geochim. Cosmochim. Acta*, *47*, 337–350.

Staudigel, H., S. R. Hart, and S. H. Richardson (1981a), Alteration of the oceanic crust: Processes and timing, *Earth Planet. Sci. Lett.*, *52*, 311–327.

Staudigel, H., K. Muehlenbachs, S. H. Richardson, and S. R. Hart (1981b), Agents of low temperature ocean crust alteration, *Contrib. Mineral. Petrol.*, *77*, 150–157.

Staudigel, H., G. R. Davies, S. R. Hart, K. M. Marchant, and B. M. Smith (1995), Large scale isotopic Sr, Nd, and O isotopic anatomy of altered oceanic crust: DSDP:ODP sites 417/418, *Earth Planet. Sci. Lett.*, *130*, 169–185.

Staudigel, H., T. Plank, B. While, and H.-U. Schmincke (1996), Geochemical fluxes during seafloor alteration of the basaltic upper oceanic crust: DSDP sites 417 and 418, in *Subduction Top to Bottom*, vol. 96, edited by G. E. Bebout et al., pp. 19–38, AGU, Washington, D. C.

Stefánsson, A., and S. Arnórsson (2002), Gas pressures and redox reactions in geothermal fluids in Iceland, *Chem. Geol.*, *190*, 251–271.

Sveinbjörnsdóttir, A. E., M. L. Coleman, and B. W. D. Yardley (1986), Origin and history of hydrothermal fluids of the Reykjanes and Krafla geothermal fields, Iceland, *Contrib. Mineral. Petrol.*, *94*, 99–109.

Sverjensky, D. (1984), Europium redox equilibria in aqueous solutions, *Earth Planet. Sci. Lett.*, *67*, 70–78.

Teagle, D. A. H., J. C. Alt, W. Bach, A. N. Halliday, and J. Erzinger (1996), Alteration of upper ocean crust in a ridge-flank hydrothermal upflow zone: Mineral, chemical, and isotopic constraints from Hole 896A, in *Proceedings of the Ocean Drilling Program, Scientific Results*, vol. 148, pp. 119–150, Ocean Drill. Program, College Station, Tex.

Teagle, D. A. H., M. J. Bickle, and J. C. Alt (2003), Recharge flux to ocean-ridge black smoker systems: A geochemical estimate from ODP Hole 504B, *Earth Planet. Sci. Lett.*, *210*, 81–89.

Teagle, D. A. H., and J. C. Alt (2004), Hydrothermal alteration of basalts beneath the Bent Hill massive sulfide deposit, Middle Valley, Juan De Fuca Ridge, *Econ. Geol.*, *99*(3), 561–584.

Teagle, D. A. H., J. C. Alt, S. Umino, S. Miyashita, N. R. Banerjee, and D. S. Wilson, and the Expedition 309/312 Scientists (2006), Expedition 309/312 summary, *Proc. Integrated Ocean Drill. Program*, *309/312*, 1–127.

Thirlwall, M. F., M. A. M. Gee, R. N. Taylor, and B. J. Murton (2004), Mantle components in Iceland and adjacent ridges investigated using double-spike Pb isotope ratios, *Geochim. Cosmochim. Acta*, *68*(2), 361–386.

Thompson, G. (1973), A geochemical study of the low temperature interaction of seawater and oceanic igneous rocks, *Trans. AGU*, *54*, 1015–1019.

Tómasson, J., and H. Kristmannsdóttir (1972), High temperature alteration minerals and thermal brines, Reykjanes, Iceland, *Contrib. Mineral. Petrol.*, *36*, 123–134.

Verma, M. P. (1992), Seawater alteration effects on REE, K, Rb, Cs, Sr, U, Th, Pb and Sr-Nd-Pb isotope systematics of Mid-Ocean Ridge basalt, *Geochem. J.*, *26*, 159–177.

Vidal, P., and N. Clauer (1981), Pb and Sr isotopic systematics of some basalts and sulfides from the East Pacific Rise at 21 N (project RITA), *Earth Planet. Sci. Lett.*, *55*, 237–246.

Wheat, C. G., M. J. Mottl, and M. Rudnicki (2002), Trace element and REE composition of a low-temperature ridge-flank hydrothermal spring, *Geochim. Cosmochim. Acta*, *66*(21), 3693–3705.

Wilson, D. S., et al. (2006), Drilling to gabbro in intact ocean crust, *Science*, *312*(5776), 1016–1020.

Wood, D. A., J. L. Joron, M. Treuil, M. Norry, and J. Tarney (1979), Elemental and Sr isotope variations in basic lavas from Iceland and the surrounding ocean floor, *Contrib. Mineral. Petrol.*, *70*, 319–339.

Zierenberg, R. A., W. C. Shanks III, and J. L. Bischoff (1984), Massive sulfide deposits at 21°N, East Pacific Rise: Chemical composition, stable isotopes, and phase equilibria, *Geol. Soc. Am. Bull.*, *95*, 922–929.

Zierenberg, R. A., et al. (1988), The deep structure of a sea-floor hydrothermal deposit, *Lett. Nat.*, *392*, 485–488.

Zindler, A., S. R. Hart, F. A. Frey, and S. P. Jakobsson (1979), Nd and Sr isotope ratios and rare earth element abundances in Reykjanes Peninsula basalts—Evidence for mantle heterogeneity beneath Iceland, *Earth Planet. Sci. Lett.*, *45*, 249–262.